ACTIVE SENSING OF VISUAL AND TACTILE STIMULI BY BRAIN-BASED DEVICES

A. K. Seth, J. L. McKinstry, G. M. Edelman, and J. L. Krichmar

The Neurosciences Institute,

10640 John Jay Hopkins Drive, San Diego, CA 92121

Email: seth@nsi.edu,

Keywords: Behaviour, categorization, conditioning, embodiment, plasticity, value systems.

Abstract

We describe the construction and performance of 'brain-based devices' (BBDs), physical devices whose behaviour is controlled by simulated nervous systems modelled on vertebrate neuroanatomy and neurophysiology, that carry out perceptual categorization and selective conditioning to visual and textural stimuli. BBDs take input from the environment through on-board sensors including cameras, microphones and artificial whiskers, and take action based on experiential learning. BBDs have a large-scale neural simulation, a phenotype, a body plan, and the means to learn through autonomous exploration. Key neural mechanisms in the present BBDs include synaptic plasticity, reward or value systems, reentrant connectivity, the dynamic synchronization of neuronal activity, and neuronal units with spatiotemporal response properties. With our BBDs, as with animals, it is the interaction of these neural mechanisms with the sensorimotor correlations generated by active sensing and self motion that is responsible for adaptive behaviour. BBDs permit analysis of activity at all levels of the nervous system during behaviour, and as such they provide a rich source of heuristics for generating hypotheses regarding brain function. Moreover, by taking inspiration from systems neuroscience, BBDs provide a novel architecture for the design of neuromorphic systems.

1. Introduction

Perceptual categorization of information sampled in different sensory modalities presents a difficult and unsolved task in robotics. In contrast, biological systems categorize complex sensory information and take the appropriate motor actions seemingly easily and naturally. In this paper we show how brain-based devices (BBDs), robotic devices whose construction is based on principles of neuroanatomy and neurophysiology, are able to categorize sensory information in both visual and haptic domains. We describe the construction and performance of two recent BBDs. The first, Darwin VIII, discriminates targets from distracters in complex visual scenes containing multiple objects with overlapping features, and therefore solves the problem of visual binding or scene segmentation [1]. The second, Darwin IX, uses custom-built artificial whiskers to navigate its environment and to categorize distinct textures. In both cases, successful perceptual categorization is demonstrated behaviourally by the acquisition of selective conditioned responses.

A BBD is a physical device whose behaviour is controlled by a simulated nervous system. Over the last 12 years, we have constructed a series of BBDs designated the Darwin automata [2-6]. All BBDs that we have constructed have the following attributes: 1) An embodied morphology that allows for active exploration in a real-world environment, including sensors such as cameras, microphones, proximity sensors, and artificial whiskers. 2) A neural simulation to control the BBD's behaviour, incorporating detailed neuroanatomy and neurophysiology based on vertebrate nervous systems. 3) A value system that signals the salience of environmental cues and that modulates plasticity in the nervous system resulting in modification of the device's behaviour. These features

result in systems that generalize signals from the environment into perceptual categories and that adapt their behaviour via conditioning to become increasingly successful in coping with their environment.

Our BBDs are not programmed by instruction like computers, but instead, like biological systems they operate according to selectional principles [7]. BBD simulations therefore tend to require large-scale networks of neuronal elements that reflect the brain's anatomy, physiology, and the dimensionality of the sensory input. This design strategy differs fundamentally from artificial intelligence approaches which are based on data representation, rule-driven algorithms, and the manipulation of formal symbol systems [8, 9].

Key neural mechanisms that give rise to the capabilities of our BBDs include synaptic plasticity, reward or value systems, reentrant connectivity, the dynamic synchronization of neuronal activity, and neuronal units with spatiotemporal response properties. In order to better understand the operation of these mechanisms, we correlate observed behaviour with detailed recordings of all neuronal responses and synaptic changes, data which would be impossible to obtain from comparable animal experiments.

Other groups have adopted approaches similar to the BBD methodology, for example using robots to explore the role of neuromodulation [10], or to analyse the acqusition of event representations via behavioral interactions with an environment [11, 12]. With regard to the categorization of visual and haptic sensory data, related work in robotics has analyzed the role of haptic manipulation and autonomous behaviour in visual object identification [13-15], and studies of whisker-based perception have explored shape reconstruction, contact point localistion, texture discrimination by a fixed whisker

array, and obstacle avoidance by a mobile robot [16-20]. The present BBDs differ from these studies by their incorporation of detailed neuroanatomy and neurophysiology, and by their emphasis on autonomous behavior. As a result, our BBDs provide general mechanisms, inspired by neuroscience, for the binding of sensory features into perceptual objects, and for the spatiotemporal transformation of whisker-based haptic sensing into perceptual categories. These mechanisms not only provide insight into brain function, but also suggest methodologies that can be incorporated into neuromorphic system design.

2. Visual Binding via Reentry and Synchrony by Darwin VIII.

Discrimination among multiple objects in a scene requires mechanisms to associate features belonging to individual objects while distinguishing distinct objects. This problem of scene segmentation, or visual binding [1, 21], remains unresolved in neuroscience and challenging from the perspective of computational vision systems. We designed Darwin VIII to investigate if the selective synchronization of reentrantly connected neuronal groups could segment a visual scene into perceptual categories that provide a basis for selective conditioning to visual objects.

A previous computational model of visual binding through synchronous activity via reentry demonstrated the ability to make simulated saccades to preferred visual objects in a virtual scene [22]. This model included nine functionally segregated simulated cortical visual areas, as well as reward and motor systems, and its performance showed that reentrant connections within and among areas facilitated the recognition and discrimination of multiple visual objects. However, despite showing the capabilities of reentrant circuits, the model had several limitations. For example, the stimuli used were taken from a limited set and were of uniform scale. Furthermore, its behaviour did not emerge in a rich and noisy environment of the kind confronted by behaving organisms or other autonomous physical devices.

To address these limitations we constructed Darwin VIII, a BBD which explores a real-world environment and autonomously approaches and views multiple objects that share visual features. In our experiments, Darwin VIII is conditioned to prefer one target object over multiple distracters, by associating the visual target with an innately preferred auditory cue. It demonstrates this preference behaviourally by orienting toward the target.

Darwin VIII's simulated nervous system consists of different neural areas analogous to cortical and sub-cortical counterparts in the vertebrate brain. These areas contain neuronal units, each of which has a mean firing rate, which roughly corresponds to the activity of 100 real neurons, as well as a firing phase, which specifies the relative timing of this activity (see *Neuronal Dynamics*, below). This neuronal model provides temporal specificity without incurring the computational costs associated with modelling spiking neurons in real-time.

Simulated synaptic connections follow known vertebrate neuroanatomical projections and include extensive reentrant connectivity within and among neural areas. Reentry, which refers to the existence of multiple parallel bidirectional connections among neural areas, is distinct from feedback, which in a strict engineering sense involves the recycling of an explicit error signal to an input [23]. In Darwin VIII, reentrant connections among neuronal units encourage phase convergence and therefore lead to the emergence of neural synchrony. Observations of Darwin VIII show that dynamic synchronization via reentry provides a plausible mechanism for visual binding and thus also for categorization and selective conditioning to visual objects in complex visual scenes. The neural mechanisms incorporated into Darwin VIII may therefore be useful for enabling neuromorphically designed systems to perform scene segmentation.

2.1 Darwin VIII: Construction and Experimental Paradigm

Physical Device

Darwin VIII consists of a mobile robotic base containing a CCD camera, microphones, IR proximity sensors, and a cluster of workstations that run the simulated nervous system and control the device's behaviour (Fig. 1). One of the workstations receives visual input via RF video transmission from a CCD camera mounted on the mobile base. The workstation also receives auditory and infrared detector information, and transmits motor and actuator commands via an RF modem. A microcontroller (PIC17C756A) onboard the base samples input and status from the sensors and controls RS-232 communication between the robotic base and the workstations.

[Figure 1 Approximately Here]

Simulated Nervous System

Darwin VIII's simulated nervous system contains regions analogous to the vertebrate nervous system, for vision, tracking, audition, and value (see Fig. 2). The nervous system contains 28 neural areas, 53,540 neuronal units, and ~1.7 million synaptic connections. It has an extensive neuroanatomy with reentrant connectivity within and among neural areas.

[Figure 2 Approximately Here]

Visual System. The visual system is modelled on the primate ventral visual pathway (in our model *V1*→*V2*→*V4*→*IT*), in which neurons in successive areas have progressively larger receptive fields [24].

Visual stimuli are input to the visual system by a CCD camera that send 320x240 pixel RGB video images, via an RF transmitter, to an ImageNation PXC200 frame grabber attached to one of the workstations running the neural simulation. The image is spatially averaged to produce an 80x60 pixel image. Gabor filters are used to detect edges of vertical, horizontal, and diagonal (45 degrees and 135 degrees) orientations. Colour filters (red positive center with a green negative surround, or red negative center with a green positive surround) are also applied to the image.

Neuronal units in the various *V1* sub-regions (*V1-red*, *V1-green*, *V1-vertical*, *V1-horizontal*, *V1-diagonal-left, V1-diagonal-right)* take input directly from the corresponding filters. Sub-regions of *V1* project topographically to corresponding sub-regions of *V2*. Area *V2* has both excitatory and inhibitory reentrant connections within and among its sub-regions. Each *V2* sub-region projects to a corresponding *V4* sub-region topographically but broadly, and *V4* sub-regions project back to the corresponding *V2* sub-regions with non-topographic reentrant connections. The reentrant connectivity within and among sub-regions of *V4* is similar to that in *V2*. *V4* projects non-topographically to *IT* so that each neuronal unit in *IT* receives input from three *V4* neuronal units randomly chosen from three different *V4* sub-regions. *IT* neuronal units project to other *IT* neuronal units through plastic connections, and back to *V4* through non-topographic reentrant connections.

Tracking System. The activity of area *C* dictates where Darwin VIII directs its camera gaze. Each neuronal unit in area *C* has a receptive field which matches its preferred direction, and activity predominately on the left (right) side of *C* causes Darwin VIII to turn towards the left (right). Areas *A-left* and *A-right* have strong excitatory projections to the respective sides of *C* causing Darwin VIII to orient towards a sound source. *V4* projects topographically to *C,* its activity causing Darwin VIII to center its gaze on a visual object. Both *IT* and the value system *S* project to *C*, and plastic connections in the pathways *IT*→*C* and *IT*→*S* facilitate target selection by creating a bias in activity reflecting salient perceptual categories (see *Value System,* below).

Auditory System. Areas *Mic-left* and *Mic-right* are activated whenever the corresponding microphones detect a sound of sufficient amplitude within a specified frequency range. These areas project respectively to areas *A-left* and *A-right*.

Microphone input is amplified and filtered in hardware on board the device. An RMS (root mean square) chip measures the amplitude of the signal and a comparator chip produces a square waveform which allows frequency to be measured. Every millisecond, the onboard microcontroller calculates the overall microphone amplitude by averaging the current signal amplitude measurement with the previous three measurements; this value is normalized in software to range from 0 to 1. The microcontroller calculates the frequency of the microphone signal at each time point by inverting the average period of the last eight square waves. The frequency and amplitude of each microphone is sent to the workstation cluster every 100ms.

Mic-left and *Mic-right* respond only to tones between 2.9 and 3.5 kHz having an amplitude of at least 0.4. The activity of the single neuronal unit in *Mic-left* or *Mic-right* is given by $s_i^{mic}(t+1) = \tanh(0.9\, s_i^{mic}(t) + 0.1\, a_i^{mic})$, where $s_i^{mic}(t)$ is the previous mean firing rate value of a neuronal unit *i* in *Mic-left* or *Mic-right* (see *Neuronal Dynamics,* below), and a_i^{mic} is the current amplitude of the microphone output. This equation smooths out spurious noise in the auditory signal.

Value System. Activity in the simulated value system (Area *S*, Fig. 2) signals the occurrence of salient sensory events and this activity contributes to the modulation of plastic connection strengths in pathways *IT→S* and *IT→C*. Initially, *S* is activated by sounds detected by Darwin VIII's auditory system (see *A-left→S* and *A-right→S* in Fig. 2). Activity in *S* is analogous to that of ascending neuromodulatory systems in that it is triggered by salient events, influences large regions of the simulated nervous system (see *Synaptic Plasticity,* below), and persists for several cycles [25-27]. In addition, due to its projection to the tracking area *C*, area *S* has a direct influence on behaviour. In Darwin VIII, as in other BBDs, value-dependent plasticity is a key neural mechanism supporting the acquisition of selective behaviours.

Neuronal Dynamics

The state of each neuronal unit in Darwin VIII is determined by a mean firing rate variable (*s*), which corresponds to the average activity of a group of roughly 100 real neurons over 100 milliseconds, and a phase variable (*p*), which specifies the relative timing of this activity (see *Neuronal Unit Activity and Phase,* below).

Synaptic connections are set to be either voltage-independent or voltage-dependent, either phase-independent or phase-dependent, and either plastic or non-plastic. Whereas voltage-independent connections provide synaptic input regardless of post-synaptic state, voltage-dependent connections require postsynaptic activity to be activated [28]. Phase-dependent connections influence both the activity and the phase of post-synaptic neuronal units, whereas phase-independent connections influence only the activity. All synaptic pathways in Darwin VIII are phase-dependent except those involved in motor output (*A-left/A-right→C*, *C↔C*) or sensory input (*Mic-left/Mic-right→A-left/A-right, A-left↔A-right*, *V1→V2*) since signals at these interfaces are defined by magnitude only. Plastic connections are either value-independent or value-dependent, as described below.

Neuronal Unit Activity and Phase. The mean firing rate (s) of each neuronal unit ranges from 0 (quiescent) to 1 (maximal firing). The phase (p) is divided into 32 discrete bins representing the relative timing of activity by an angle ranging from 0 to 2π. The state of a neuronal unit is updated as a function of its current state and contributions from all inputs. The voltage-independent input to unit i from unit j is:

$$A_{ij}^{VI}(t) = c_{ij}\, s_j(t) \tag{1}$$

where $s_j(t)$ is the activity of unit j, and c_{ij} is the connection strength from unit j to unit i. The voltage-independent postsynaptic influence on unit i is calculated by convolving this value into a cosine-tuning curve:

$$POST_i^{VI} = \sum_{l=1}^{M}\sum_{j=1}^{N_l}\left(A_{ij}^{VI}(t)\sum_{k=1}^{32}\left(\frac{\cos\left((2\pi/32)(k-p_j(t))\right)+1}{2} \right)^{tw} \right) \tag{2}$$

where M is the number of different anatomically defined connection types (see Table 2); N_l is the number of connections of type M projecting to unit i; $p_j(t)$ is the phase of neuronal unit j at time t; and tw is the tuning width, which in our experiments is set to 10 so that the tuning curve is relatively sharp (~5 phase bins).

The voltage-dependent input to unit i from unit j is:

$$A_{ij}^{VD}(t) = \Phi\left(POST_i^{VI}\left(p_j(t)\right)\right) c_{ij}\, s_j(t), \text{ where } \Phi(x) = \begin{cases} 0; & x < \sigma_i^{vdep} \\ x; & otherwise \end{cases} \quad (3)$$

where σ_i^{vdep} is a threshold below which voltage-dependent connections have no effect (see Table 1).

The voltage-dependent postsynaptic influence on unit i is:

$$POST_i^{VD} = \sum_{l=1}^{M}\sum_{j=1}^{N_l}\left(A_{ij}^{VD}(t)\sum_{k=1}^{32}\left(\frac{\cos\left((2\pi/32)(k-p_j(t))\right)+1}{2} \right)^{tw} \right) \quad (4)$$

The phase-independent activation into unit i from unit j is:

$$A_{ij}^{PI}(t) = c_{ij}\, s(t). \quad (5)$$

The phase-independent postsynaptic influence on unit i is:

$$POST_i^{PI}(p) = \sum_{l=1}^{M}\sum_{j=1}^{N_l}\left(\frac{A_{ij}^{PI}(t)}{32} \right) \quad (6)$$

A new phase, $p_i(t+1)$, and activity, $s_i(t+1)$ are chosen based on a distribution created by linearly summing the post-synaptic influences on neuronal unit i (see Fig. 3):

$$POST_i = \sum_{j=1}^{N_{VI}} POST_j^{VI} + \sum_{k=1}^{N_{VD}} POST_k^{VD} + \sum_{l=1}^{N_{PI}} POST_l^{PI} \quad (7)$$

[Figure 3 Approximately Here]

The phase threshold, σ_i^{phase}, of the neuronal unit is subtracted from the distribution $POST_i$ and a new phase, $p_i(t+1)$, is chosen with a probability proportional to the resulting distribution (Fig. 3; bottom row). If no inputs are above the phase threshold, $p_i(t+1)$ is chosen at random. The new activity for the neuronal unit is the activity level at the newly chosen phase, which is then subjected to the following activation function:

$$s_i(t+1) = \phi\left(\tanh\left(g_i\left(POST_i\left(p_i(t+1)\right) + \omega s_i(t)\right)\right)\right), \text{ where } \phi(x) = \begin{cases} 0; & x < \sigma_i^{fire} \\ x; & otherwise \end{cases} \quad (8)$$

where ω determines the persistence of unit activity, g_i is a scaling factor, and σ_i^{fire} is a firing threshold (see Table 1).

[Table 1 Approximately Here]

[Table 2 Approximately Here]

Synaptic Plasticity. Plastic synaptic connections are either value-independent (see *IT*→*IT* in Fig. 2) or value-dependent (see *IT*→*S*, *IT*→*C* in Fig. 2). Both types of plasticity are based on a modified BCM learning rule [29] in which synapses between neuronal units with strongly correlated firing phases are potentiated and synapses between neuronal units with weakly correlated phases are depressed (see Fig. 2, inset). Value-independent synaptic changes in c_{ij} are given by:

$$\Delta c_{ij}(t+1) = \eta\, s_i(t) s_j(t) BCM(\Delta p) \tag{9}$$

where $s_i(t)$ and $s_j(t)$ are activities of post- and pre-synaptic units, respectively, η is a fixed learning rate, and $\Delta p = \dfrac{\cos\left((2\pi/32)(p_i(t) - p_j(t))\right)+1}{2}$, where $p_i(t)$ and $p_j(t)$ are the phases of post- and pre-synaptic units. The function *BCM* is implemented as follows (parameters are given in Table 2, $\rho = 6$ throughout):

$$BCM(\Delta p) = \begin{cases} 0; & \Delta p < \theta_1 \\ k_1(\theta_1 - \Delta p); & \theta_1 \le \Delta p < (\theta_1 + \theta_2)/2 \\ k_1(\Delta p - \theta_2); & (\theta_1 + \theta_2)/2 \le \Delta p < \theta_2 \\ k_2 \tanh(\rho(\Delta p - \theta_2))/\rho; & \textit{otherwise} \end{cases} \tag{10}$$

For value-dependent synaptic plasticity, connections terminating on neuronal units that are in phase with the value system are potentiated, whereas those terminating on units out of phase with the value system are depressed. The synaptic change for value-dependent synaptic plasticity is given by:

$$\Delta c_{ij}(t+1) = \eta\, s_i(t) s_j(t) BCM(\Delta p) V(t) BCM_v(\Delta p_v) \tag{11}$$

where $V(t)$ is the mean activity level in the value area S at time t. Note that the BCM_v function uses the phase difference between the value area S and the post-synaptic neuronal unit ($\Delta p_v = \dfrac{\cos\left((2\pi/32)(p_V(t) - p_i(t))\right)+1}{2}$) as input. When both *BCM* and BCM_v return a negative number, BCM_v is set to 1 to ensure that the synaptic connection is

not potentiated when both the pre-synaptic neuronal unit and value system are out of phase with the post-synaptic neuronal unit.

Simulation Cycle Computation. During each simulation cycle of Darwin VIII, sensory input is processed, the states of all neuronal units are computed, the connection strengths of all plastic connections are determined, and motor output is generated. In our experiments, execution of each simulation cycle requires approximately 100 milliseconds of real time. The simulated nervous system is implemented on a Beowulf cluster of twelve, 1.4 GHz Pentium IV workstations running Message Passing Interface (MPI) parallel software under the Linux operating system.

Experimental Paradigm

Darwin VIII's environment consists of an enclosed area with black walls (see Fig. 4). Various pairs of shapes from a set consisting of a green diamond, a green square, a red diamond, and a red square are hung on two opposite walls. The floor contains a boundary made of reflective construction paper. Detection of this boundary by Darwin VIII's downward-facing IR sensor evokes a reflexive avoidance movement. Near the boundary of walls containing visual shapes, infrared emitters (IR) on one side of the room are paired with IR receivers containing a speaker on the other side. If Darwin VIII breaks either beam, a tone is emitted which elicits an orientation movement towards the source of the sound.

[Figure 4 Approximately Here]

Experiments were divided into training and testing stages. During training, Darwin VIII explored its enclosure for 10,000 simulation cycles, corresponding to ~24 approaches to the various pairs of visual shapes. Each pair contained a 'target' shape and a 'distracter' shape, with the target always closest to the speaker so that responses to the speaker caused Darwin VIII to orient towards the target. Distracters were deliberately designed to share attributes with the target, for example, when the red diamond was the target, a red diamond/red square pair was hung on one wall, and a red diamond/green diamond pair was hung on the other wall. We exchanged the side of the distracters every sixth viewing of a pair.

During testing, the speakers were turned off, and Darwin VIII was allowed to explore its enclosure for 15,000 simulation cycles during which the target was paired with each of the three possible distracters for 5,000 cycles each. Training and testing was repeated with three different Darwin VIII "subjects" using each of the four shapes as a target. Each subject possessed a unique simulated nervous system as consequence of random initialization in both the microscopic details of connectivity between individual neuronal units and the initial connection strengths between those units (see Fig. 2 and Table 2).

2.2 Darwin VIII: Visual Binding Results

Selective Conditioning to Targets

Successful conditioning was assessed by the fraction of time for which the target was centered in Darwin VIII's visual field during each approach to a pair of visual objects, in the absence of auditory cues.

[Figure 5 Approximately Here]

All subjects successfully tracked the four different targets over 80% of the time (Fig. 5A). Successful performance on this task is not trivial. Targets and distracters appeared in the visual field at many different scales and at many different positions as Darwin VIII explored its environment. Moreover, because of shared properties, targets could not be reliably distinguished from distracters on the basis of colour or shape alone. Thus, the behaviour of Darwin VIII demonstrates visual categorization and selective conditioning in a rich visual environment.

To investigate the importance of the presence of reentrant connections in the model, certain inter-areal reentrant connections were lesioned at different stages of the experimental paradigm. In one case, previously trained subjects were retested after lesioning. In a second, reentrant connections were lesioned in both training and testing stages. Lesions were applied to a subset of inter-areal excitatory reentrant connections (see projections marked with an 'X' in Figure 2 and in Table 2), which had the effect of transforming the simulated nervous system into a 'feed-forward' model of visual processing. To compensate for the reduction in activity due to these lesions, neuronal

unit outputs in areas *V2* and *V4* were amplified (see Table 1). Figure 5B shows that subjects with intact reentrant connections performed significantly better than either lesioned group (Wilcoxon Ranksum test; $p < 0.01$). The decrease in performance observed in the absence of reentry indicates that reentrant connections are essential for behaviour above chance in the discrimination task.

Neural Dynamics During Behaviour

During the behaviour of an intact Darwin VIII subject, we observed circuits comprised of synchronously active neuronal groups which were distributed throughout different areas in the simulated nervous system. Multiple objects were distinguishable by the differences in phase between the corresponding active circuits. A snapshot of Darwin VIII's neural responses is given in Fig. 6, in which the device is approaching a red diamond target and a green diamond distracter towards the end of a training session. Each pixel in each neural area represents the activity (brightness) and phase (colour) of a single neuronal unit. The figure shows two neural circuits differentiated by their distinct phases and which were elicited respectively by the red diamond and the green diamond. The neuronal units making up these circuits were distributed throughout the nervous system. As shown in the figure, Darwin VIII had not yet reached the beam that triggers the speaker to emit a tone. The activity of area *S* was nonetheless in phase with the activity in areas *V2* and *V4* corresponding to the target, and is therefore predictive of the target's saliency or value. Area *IT* has two patterns of activity, indicated by the two different phase colours, which reflect two perceptual categories. The increased activity in area *C*

on the side of the target is causing Darwin VIII to orient towards the target (i.e. the red diamond).

[Figure 6 Approximately Here]

Value System Activity During Conditioning

As a result of value-dependent synaptic plasticity during conditioning, the visual attributes of target objects become predictive of value. Fig. 7 illustrates neural dynamics from a single intact Darwin VIII subject during both early (left panel) and late (right panel) stages of conditioning. Each panel shows the distribution of neuronal unit phases in the corresponding area over time. A gray scale indicates the proportion of neuronal units in each area at a particular phase (white represents no neuronal units, black represents the maximal proportion of neuronal units). During early conditioning, the onset of the tone evokes significant changes in neural dynamics. Before tone onset, area *S* is inactive and areas *IT* and *C* show bimodal phase distributions with the distinct peaks corresponding to the two objects in Darwin VIII's visual field. When the tone is present (indicated by the solid line at the bottom of the panel), *S* is strongly active in phase with visual system activity corresponding to the target, causing potentiation of active synapses in the pathways *IT*→*C* and *IT*→*S*, and activity in areas *IT* and *C* is also strongly biased toward this phase, causing Darwin VIII to orient to the target.

[Figure 7 Approximately Here]

After conditioning, as a result of this value-dependent plasticity, the target visual features become associated with value such that activity in *S* now *precedes* tone onset (right panel). In fact, *S* now responds to the target stimulus as soon as the stimulus appears in Darwin VIII's visual field, and this activity facilitates a bias in the activity of areas *IT* and *C* in favor of the target. This shift in the timing of value-related activity is similar to the 'temporal-difference' learning rule in that the conditioned stimulus (the target) becomes predictive of value [30-32].

2.3 Darwin VIII: Visual Binding Summary

Visual binding in Darwin VIII occurred as a result of the dynamic synchronization of the activity of neuronal groups via reentry. In a conditioning paradigm, Darwin VIII showed selective behaviour towards target visual objects even when distracter objects, which share visual features with the target, were simultaneously present in its visual field. Reliable perceptual categorization was achieved by Darwin VIII despite the continual changes in the scale and position of stimuli in the visual field resulting from self-generated movement.

Key mechanisms incorporated into Darwin VIII were reentrant connections within and among areas, neuronal units with both a mean firing rate and a relative firing phase, and a value system modulating synaptic plasticity. The operation of these mechanisms, in conjunction with the sensorimotor correlations generated by self-motion, enabled Darwin VIII to categorize visual objects, bind the features of visual objects, segment a scene, and demonstrate selective behaviour in a rich real-world environment.

3. Texture Discrimination and Aversion Conditioning by Darwin IX

Haptic sensory information provided by mystacial vibrissae (whiskers) allows the rat to discriminate among different textures in its environment [33, 34]. Although whisker-based perception lacks the fine resolution and long range of vision, whiskers have the advantage of allowing navigation and discrimination in the dark. Despite this advantage, whisker-based perception has received much less attention from roboticists than has vision (although see [16-19]).

To explore how haptic data may be integrated into perceptual categories by a brain-based device, we equipped Darwin IX with artificial whiskers and a simulated nervous system based on the neuroanatomy of the rat somatosensory system. We tested the hypothesis that neuronal units with time-lagged response properties, together with value-based modulation of synaptic plasticity, provide a plausible neural mechanism for the spatiotemporal transformations of whisker input needed for both texture discrimination and selective conditioning to textures.

In our experiments with Darwin IX, the device autonomously explored a walled environment containing two distinct textures each consisting of patterns of pegs embedded in the walls. It became conditioned to avoid one of the textures by association of this texture with an innately aversive simulated 'foot-shock'. Darwin IX demonstrated its conditioned behaviour by freezing and then moving away from walls containing the texture corresponding to the innately aversive stimuli.

[Figure 8 Approximately Here]

3.1 Darwin IX: Construction and Experimental Paradigm

Artificial Whisker Design

Darwin IX is based on the physical platform of Darwin VIII augmented by a whisker array on each side (fig. 8A and fig. 8B). Each array consists of seven whiskers arranged in a column of three and a row of five (fig. 8A. and fig. 8B). Whisker columns supply input to the simulated nervous system, while whiskers in the rows support innate avoidance and wall-following behaviours (see *Innate Behaviour,* below).

Each whisker consists of two 4cm by 0.63cm polyamide strips, adhered back-to-back and held together with small polyamide sleeves, that are responsive to bend (Jameco, CA). These strips are typically used as strain sensors in devices such as virtual reality gloves. Each strip each has 20 resistive areas embedded regularly along its length, providing a resistance of ~10KΩ when the strip is unbent and ~50KΩ when strip is maximally bent. Each strip detects bending in only one direction, hence the back-to-back arrangement. Note that because of the regular arrangement of resistive areas, whisker signals can be generated by bending along any part of the whisker.

A sliver of spring steel (thickness 0.2mm, width 4mm) is sandwiched between each pair of polyamide strips to increase whisker stiffness and to vary the whisker lengths. In Darwin IX the longer whiskers are towards the front: The frontmost whiskers are ~21cm long, the adjacent whisker is ~19cm long, the whiskers in the column are ~14cm long, and the backmost whisker is ~12.5cm long (fig. 8B). All whiskers are oriented at ~90 degrees with respect to the anterior-posterior axis of Darwin IX, apart

from the frontmost whiskers which are oriented at ~45 degrees with respect to this axis to facilitate detection of walls and corners in Darwin IX's environment.

Voltage signals from each pair of strips (i.e. a whisker) are converted to a single signal ranging from 0V (maximum deflection in one direction) to 5V (maximum deflection in the opposite direction). These voltages are converted into digital signals, ranging from 0 to 256, by a 12-bit analog-to-digital converter at a sample rate of 40Hz. During each simulation cycle of Darwin IX, which lasts 100ms, a 'packet' of 4 values for each whisker is received by Darwin IX's neural simulation. For whisker k at simulation cycle t, the corresponding packet is $[w_{k1}(t),\ w_{k2}(t),\ w_{k3}(t),\ w_{k4}(t)]$, where $w_{k4}(t)$ is the most recent value. We refer to the first value in each packet, $w_{k1}(t)$, as the 'current whisker value'.

Innate Behaviour

As with previous Darwin automata, Darwin IX is equipped with innate behavioural responses. The default behaviour of Darwin IX is to move forward in a straight line at a speed of ~8cm/sec. If Darwin IX approaches a wall head-on to within a distance of ~4cm, an avoidance response is triggered by either of two IR sensors, one facing front-left, and the other facing front-right: The device stops, backs up (~10cm), and then turn ~30 degrees away from the wall before resuming default behaviour.

Darwin IX has an innate freezing/escape response which is triggered by a simulated foot-shock (see *Experimental Environment*, below). This responses consists of continued movement for 55 simulation cycles (~5.5s), freezing for 40 cycles (~4s) then a

turn away from the nearest wall (as determined by the whisker array most recently deflected) by an angle randomly chosen from the interval [π/4 - 3π/4].

Darwin IX also has an innate wall-following capability such that, on encountering a wall, the device moves parallel to the wall at a distance suitable for the detection of embedded textures. Wall following is based on signals from three whiskers on each side (fig. 8A); the rearmost (BK), the lowest of the vertical stack (MD), and the frontmost (FT). For each of these whiskers, a running average of the current whisker value ($\overline{w}$) is maintained over 75 simulation cycles. This average is updated at every cycle except when the current whisker value differs by more than 10 from the corresponding average (signifying whisker deflection; recall that the range of the current whisker value is 0-255). For each whisker on each side, a 'deflection' value *wd* is calculated as:

$$wd_{BK}(t) = \left| w_{BK1}(t) - \overline{w}_{BK}(t) \right| \tag{12}$$

$$wd_{MD}(t) = \left| w_{MD1}(t) - \overline{w}_{MD}(t) \right| \tag{13}$$

$$wd_{FT}(t) = \left| w_{FT1}(t) - \overline{w}_{FT}(t) \right| \tag{14}$$

Wall-following of a left(right) wall is triggered when any deflection value for the left(right) whiskers exceeds 15. During each cycle of wall-following, adjustments are made to the speed of the wheel furthest from the wall (the contralateral wheel); the other (ipsilateral) wheel remains at the default speed of W_{def} = 35. Contralateral wheel speeds are set using:

$$W_{speed} = W_{def} - back - mid - front \tag{15}$$

where $front = 0.25(wd_{FT})$, $mid = g_w(wd_{MD} - \varphi_w)$, and $back = g_w(wd_{BK} - \varphi_w)$, and where *mid* and *back* were bounded in the range ±5, and g_w and φ_w are scaling factors

chosen according the physical response characteristics of the whiskers (see Table 3). Additionally, g_w varies according to the sign of the corresponding *wd* such that there is a bias in favor of turning towards a wall (see Table 3, columns 4 and 5).

[Table 3 Approximately Here]

Neuroanatomy

Darwin IX's simulated nervous system comprises 17 areas, 1101 neuronal units, and ~8400 synaptic connections (fig. 9). It contains areas analogous to the somatosensory pathway in the rat brain, specifically the (ventromedial) nuclei of the thalamus, and primary and secondary somatosensory areas (in our model, *Th*→*S1*→*S2*). Areas *S1* and *Th* are subdivided into left (*L*) and right (*R*) regions and further into 'top' (*T*), 'middle' (*M*) and 'bottom' (*B*) subregions, such that each subregion receives input from a single whisker in the column on the corresponding side. These subregions are analogous to so-called whisker 'barrels' (in rat S1) and 'barreloids' (in rat thalamus); as in Darwin IX, each whisker barrel/barreloid in the rat contains cells that respond preferentially to a specific whisker [35, 36].

[Figure 9 Approximately Here]

Neuronal units in area *Th* respond to whisker input with unit-specific time delays (see *Neuronal Dynamics*, below). These units project topographically to the corresponding units in *S1*. Each barrel of *S1* has local inhibitory connections which serve

to increase the activity contrast among neuronal units. All barrels in *S1* project to area *S2* such that each neuronal unit in *S2* takes input from 3 neuronal units, each of which is in a different barrel of either the left sub-area or the right sub-area of *S1*. This arrangement, which is similar to that used between *V4* and *IT* in Darwin VIII, ensures that synaptic input to a neuronal unit in *S2* is sparse and balanced. A deflection of a particular sequence of Darwin IX's whiskers leads to a spatiotemporal pattern of activity in *S2*. Such a dynamic sequence is comparable to that observed in the rat brain [37].

Darwin IX's nervous system also contains areas supporting the acquisition of conditioned aversion (see *Aversive Conditioning*, below). Area *FS* is activated by detection of a 'foot-shock' (see *Experimental Environment*, below), and projects to areas *S, Amy,* and M_{ave}. Area *S* is a value system similar to the corresponding area in Darwin VIII. Area *Amy* is analogous to the amygdala, a neural area which has been widely implicated in the acquisition of conditioned fear [38, 39]. Area M_{ave} is analogous to a motor cortical area, activity in which elicits an innate aversive freezing/escape response.

Whisker Input and Lag Cells

Whisker input to the neural simulation is provided by transforming each whisker packet into a vector of 'difference values' according to:

$$diff_k(t) = [\, w_{k4}(t) - w_{k3}(t),\ w_{k3}(t) - w_{k2}(t),\ w_{k2}(t) - w_{k1}(t),\ w_{k1}(t) - w_{k4}(t\text{-}1) \,] \qquad (16)$$

for whisker k at simulation cycle t. These values from the whisker in each column provide input to the corresponding barreloids of area *Th*.

Each barreloid in area *Th* contains 20 'lag' cells; neuronal units which have time-lagged response properties similar to those found in the lateral geniculate nucleus of the cat [40, 41]. Each lag cell is characterized by an internal state (s_i^{in}), an output (s_i), and a cell-specific lag parameter set to be $\psi_i = \frac{0.2}{i}, i \in \{1,2,\cdots,20\}$ for cell i in each barreloid. When triggered by a whisker deflection, the internal s_i^{in} state of cell i in the corresponding barrel increases at rate determined by ψ_i. When this internal state reaches a threshold, the cell begins to emit an output signal and s_i^{in} is reset to zero. Because of differences in ψ_i among lag cells, cells in a barreloid fire with a range of delays, from 1 to 20 simulation cycles, following deflection of the corresponding whisker (see Fig. 9; inset).

Specifically, s_i^{in} in the barreloid corresponding to whisker w_k, is updated according to:

$$s_{ki}^{in}(t+1) = \begin{cases} 0.2; & s_{ki}^{in}(t) < 0.2,\ \overline{diff_k}(t) > 3.0 \\ 0; & s_{ki}^{in}(t) \geq \sigma_i^{fire} \\ (1+\psi_i)(s_{ki}^{in}(t)); & otherwise \end{cases} \quad (17)$$

where $\overline{diff_k}(t)$ is the average $diff_k(t)$ value (a value exceeding 3.0 signifies a whisker deflection), and σ_i^{fire} is a firing threshold (see Table 4).

The output s_{ki} is calculated using:

$$s_{ki}(t+1) = \begin{cases} \tanh\left(10\left(\omega_i(s_{ki}(t))\right)\right); & s_{ki}^{in}(t) < \sigma_i^{fire} \\ \tanh\left(10\left(\omega_i(s_{ki}(t)) + (1-\omega_i)s_{ki}^{in}(t)\right)\right); & otherwise \end{cases} \quad (18)$$

where ω_i determines the persistence of unit activity from one cycle to the next (see Table 4). This value is fed as input into neuronal units in the corresponding barrels of *S1*.

Neuronal Dynamics

With the exception of the lag cells in area *Th*, neuronal units in Darwin IX use the same mean firing rate model as in Darwin VIII, but without the phase parameter (phase is set to zero for all neuronal units in the model). The properties of synaptic connections in Darwin IX are given in Table 5.

Synaptic Plasticity

Synaptic plasticity in Darwin IX acts to strengthen connections between simultaneously active neuronal units in areas *S2* and *Amy*, according to the following rule:

$$\Delta c_{ij}(t+1) = \eta\, s_j(t) BCM(s_i(t))(V(t) - 0.1) \tag{19}$$

where η is a fixed learning rate, $s_i(t)$ and $s_j(t)$ are the activities of the post- and pre-synaptic units respectively, $V(t)$ is the mean activity in area *S*, and *BCM*() is as described previously (see *Darwin VIII: Construction and experimental paradigm*, above) except that post-synaptic activity is used as input rather than the phase-difference between post- and pre-synaptic units. The term $(V(t) - 0.1)$ causes depression of plastic connections in the absence of value system activity.

[Table 4 Approximately Here]

[Table 5 Approximately Here]

Aversive Conditioning.

Synaptic plasticity supports conditioned aversion to texture as follows. Area *S* maintains a baseline level of activity (0.1) in the absence of input ($\sigma_i^{fire} = -0.1$; see Table 4). Detection of a simulated foot-shock (see *Experimental Environment*, below) causes neuronal units in area *FS* to produce a steady output of magnitude 1.0. This output pushes activity in area *S* above baseline, which causes potentiation of synapses onto neuronal units in area *Amy* from units in *S2* corresponding to the currently present texture (see equation (19)). Freezing/escape responses are triggered by activity in M_{ave} exceeding a threshold (0.5) as a result of input from areas *FS* and/or *Amy* (see fig. 8C). This model also supports extinction of conditioned responses: If *Amy* is activated without any corresponding foot-shock, area *S* will be inhibited such that its firing rate will drop below baseline, and currently active synapses between *S2* and *Amy* will be weakened (see equation (19)).

Experimental Environment

Fig. 10 shows the overall arrangement of Darwin IX's environment. One texture (*T1*) consists of a vertically aligned column of pegs, the other (*T2*) consists of a vertically staggered set of pegs with offsets between pegs of ~6cm (fig. 8C). Two adjacent walls contained *T1*, the other two contained *T2*, and either *T1* or *T2* can be associated with a simulated aversive foot-shock. This foot-shock is registered by Darwin IX's downward-facing IR sensor detecting reflective construction paper placed on the floor of the arena near the aversive texture. Note that Darwin IX typically travels in both clockwise and anti-clockwise directions around the environment such that the textures deflect both the

left and the right whisker arrays. Moreover, in the case of *T2*, the pattern of whisker deflection depends on the direction of travel.

[Figure 10 Approximately Here]

Experimental Protocol

Experiments were divided into training and testing stages. During training, either *T1* or *T2* was paired with foot-shock and Darwin IX autonomously explored its enclosure for 25,000 simulation cycles, corresponding to ~48 encounters with each wall and ~24 aversive responses to the simulated foot-shock. During testing, the foot-shock pads were removed and Darwin IX was allowed to explore its enclosure for 15,000 simulation cycles. Training and testing was repeated using three different Darwin IX "subjects" initialized with different random seeds, and pairing both *T1* and *T2* with foot-shock (six training/testing episodes in total). During training and testing of each subject, responses of all neuronal units were recorded and saved for analysis. The position of Darwin IX was also continuously recorded by an overhead camera that detected an array of LEDs positioned on the top surface of the device, the images from which were time-stamped for analysis.

3.2 Darwin IX: Results from Texture Discrimination Experiments

Selective Conditioning to Textures

Texture discrimination by Darwin IX subjects was assessed by monitoring trajectories during testing. Fig. 11 shows the behaviour of a single Darwin IX subject during training

in which foot-shock was paired with *T1*, and during testing, in which the foot-shock pads were removed. In each case line tracings indicate the trajectory with locations of aversive responses marked by circles. Most aversive responses, both to foot-shock and to *T1*, were in regions associated with the aversive texture. This response pattern is similar to that observed during the conditioning of animals to aversive stimuli [42].

[Figure 11 Approximately Here]

Taking into account data from all subjects reveals near perfect conditioned avoidance of aversive textures. During testing, Darwin IX subjects which were trained to avoid *T1* made aversive responses on 96.6% (S.E. = 0.18%) of encounters with *T1*. When trained to avoid *T2*, these subjects made aversive responses on 97.9% (S.E. = 0.14%) of encounters with *T2* during testing. Only 3.2% of all aversive responses during testing occurred inappropriately, i.e. in response to whisker deflections by walls or by the texture *not* associated with foot-shock.

Spatiotemporal neural activity

Darwin IX's ability to categorize textural stimuli is supported by spatiotemporal patterns of activity in *S2*. Each texture deflects whiskers in a column in a specific temporal order. The lag cells in area *Th* and neural units downstream in *S1* present a pattern of activity with both a spatial component (i.e. the particular whisker) and a temporal component (i.e. the time since deflection). *S2* responds to particular combinations of this *S1* activity.

The population response of *S2* to a texture was specific and repeatable. Fig. 12 shows representative *S2* activity patterns during testing of a Darwin IX subject. The top panels show *S2* activity during encounters of the left whisker column with *T1*. The bottom panels show encounters of the same whiskers with *T2*. While all panels show complex spatiotemporal patterns of activity, the top panels are highly similar to each other, the bottom panels are also highly similar to each other, but the top and bottom panels are dissimilar. This observation is supported quantitatively by measures of pattern similarity over time for all possible pairs, calculated as the normalized vector product (see Fig. 13). As shown in this figure, there is high similarity between activity patterns representing the same texture (solid lines), but not between activity patterns representing different textures (dashed lines).

[Figures 12 and 13 Approximately Here]

4.3 Darwin IX: Texture Discrimination Summary

Darwin IX demonstrates the ability to categorize objects based on haptic sensing and to learn behavioural responses selective to specific textures. Observations of Darwin IX show that time-lagged neuronal responses to somatosensory input together with value-dependent synaptic plasticity provide a plausible mechanism for the spatiotemporal transformations of sensory input needed for texture discrimination, and can provide a basis for selective conditioned aversion to textures.

Categorizing objects using only the information provided by whiskers involves multiple spatiotemporal transformations. The spatial patterns of textures are transformed, by self-movement, into temporal patterns of whisker deflections, which are themselves transformed into spatiotemporal patterns of neural activity in area *S2*, via a combination of the intrinsic properties of lag cells in area *Th* and the arrangement of projections in the pathway *Th*→*S1*→*S2*. As a result, neuronal units in *S2* respond to specific combinations of whisker deflections with particular post-stimulus delays. Analysis of neural activity in *S2* revealed the formation of spatiotemporal activity patterns corresponding to specific haptic perceptual categories (Fig. 12). The response properties of these units are similar to cells with complex spatiotemporal receptive fields that have been found in rat somatosensory cortex [37] as well as in cat visual cortex [43].

Texture discrimination by Darwin IX was assessed behaviourally following a paradigm based on fear conditioning in which one texture was paired with a simulated foot-shock. In this paradigm, simulated foot-shock triggers a freezing/escape response and activates a value system which modulates synaptic plasticity between *S2* and a neural area analogous to the rodent amygdala (*Amy*). Activity in *Amy* evokes a conditioned freezing and escape response via excitatory projections to M_{ave}. As a result of these interactions, Darwin IX became conditioned to avoid the aversive texture.

4. Conclusion

In this paper we have shown how brain-based devices (BBDs), based on principles of neuroanatomy and neurophysiology, are able to categorize sensory information in both visual and haptic domains. In all of our experiments, BBDs demonstrate successful categorization through the acquisition and recall of selective behaviours (i.e. conditioning paradigms that associate specific classes of stimuli with specific motor responses). Darwin VIII and Darwin IX demonstrate selective conditioning and perceptual categorization of a variety of complex stimuli. Darwin VIII discriminates objects in complex visual scenes containing multiple objects with overlapping features and orients towards preferred targets. Darwin IX categorizes textures by the spatiotemporal deflections of artificial whiskers and associates specific textures with aversive unconditioned stimuli resulting in the BBD avoiding the region of the environment containing that texture.

Although we were able to detect successful categorization and conditioning by Darwin VIII and Darwin IX solely from behavioural evidence, we correlated observed with behaviour with detailed recordings of neural responses to better understand the neural mechanisms underlying these capabilities. For example, both Darwin VIII and Darwin IX acquired selective conditioned behaviours as a result of modality-specific perceptual categorization in conjunction with value-dependent synaptic plasticity, which served to strengthen connections in certain synaptic pathways linking stimulus representations (*IT*, *S2*) to motor output (*C*, M_{ave}).

More specifically, selective conditioning by Darwin VIII required neural mechanisms to associate features belonging to individual objects while distinguishing

distinct objects [1]. Key to solving this problem of visual binding were the presence of reentrant connections within and among neural areas. In Darwin VIII, these connections support the formation of synchronously active functional circuits corresponding to perceptual categories. The formation of these circuits also required a neuronal model combining a mean activity level with a phase variable representing the relative timing of activity.

Perceptual categorization by Darwin IX involved multiple spatiotemporal transformations. First, a spatially defined stimulus (a texture) is transformed into temporally arranged sensory input as a result of whisker deflections during movement. Second, this input is reformed into spatial patterns of activity in area *S2*, corresponding to perceptual categories, as a result of the response properties of the 'lag' cells in the barrel regions of area *Th* and the connectivity in the pathway *Th*→*S1*→*S2*. The response properties of units in *S2* are analogous to cells with complex spatiotemporal receptive fields that have been found in rat somatosensory cortex.

In all cases the successful operation of these neural mechanisms -- synaptic plasticity, reentrant connectivity, dynamic synchronization, and spatiotemporally transformations -- required a close coupling between neural dynamics and behaviour. In general, neural mechanisms are both *embodied and embedded*, that is, they interact with an external environment via a morphology or body [7, 44]. For this reason, the design of BBDs involves physically instantiated devices placed into real-world environments. Such a commitment avoids the implicit assumptions that accompany computer simulations of agents and environments. For example, simulating the physical interactions between whiskers and walls would be extremely difficult without many simplifying assumptions.

Darwin IX captures the nuances of these interactions 'for free' and shows how they can provide a basis for both navigation and discrimination. Also, physical instantiation often reveals synergies between adaptive behaviour and neural mechanisms that may otherwise remain opaque. In Darwin VIII, for example, self-motion was essential for guiding synaptic plasticity to facilitate the development of invariant object recognition.

Both visual perception and haptic perception have received increasing attention from roboticists in recent years. For example, it has been shown, using a humanoid robot, that haptic manipulation of objects can facilitate visual scene segmentation [13]. Other groups have explored visual categorization by behaving robots [14, 15], and some roboticists are now describing 'cognitive' robots with – for example – multiple memory systems [45, 46]. Darwin VIII differs from these approaches by incorporating detailed neuranatomy and neurophysiology. Its reentrant neuroanatomy and phase-based neuronal model provide a general mechanism for the binding of sensory features into distinct – and simultaneously present – perceptual objects.

Artificial whiskers have been constructed and analyzed for at least 25 years [47]. Passively mounted artificial whiskers have been applied to reconstructing object shape [16], to detecting points of contact with objects [17], and to discriminating among textures [18]. Others have mounted artificial whiskers on mobile robots to support obstacle avoidance [19, 20]. Darwin IX extends these studies by showing texture discrimination using whisker arrays mounted on an autonomously behaving device. Moreover, Darwin IX's neural simulation provides a foundation for spatiotemporal pattern recognition that may underlie whisker-based perception in a variety tasks,

including landmark recognition and navigation, object recognition and localisation, as well as texture discrimination and conditioning.

The size of our neural simulations varies from the large (53,540 neuronal units in Darwin VIII) to the comparatively modest (1,101 neuronal units in Darwin IX). This variation is a function of the dimensionality of the sensory input (large for vision, smaller for whiskers) and the preservation of the relevant neuroanatomical structure. Fortunately, the BBD approach is inherently scalable: All neuronal units are updated using the same difference equations, so that an increase in the number of neuronal units in a simulation does not necessarily increase the complexity of its implementation.

The BBD approach also captures the characteristic robustness of the corresponding biological systems, in terms of component failure as well as variability in input. For example, object recognition by Darwin VIII is invariant to large changes in scale and object position, and texture discrimination by Darwin IX is robust to small variations among instances of each texture in its environment. Moreover, our observations of neural dynamics during behavior indicate that neuronal activity patterns in Darwin VIII and in Darwin IX are degenerate, i.e. different neuronal circuits can support the same behavioral output [48]. This suggests that our BBDs may be tolerant to neuronal unit failures [4].

Our BBDs provide both neuron-level and systems-level heuristics for neuromorphic design by modelling the capabilities of vertebrate nervous systems. In the wild, these systems allow animals to recognize objects with different modalities without explicit instructions and carry out selective behaviour that is crucial to their survival. They function in noisy environments and are able to generalize so that recognition is

invariant to perturbations and changes due to movement. Our BBDs show that these attributes of nervous systems may usefully be incorporated into neuromorphic devices to enable such devices to negotiate complex visual and tactile environments.

In general, higher brain function depends on the cooperative activity of the entire nervous system, reflecting its morphology, its dynamics, and its interaction with the body and the environment. The development and analysis of brain-based devices provides a methodology for tracing these interactions and the Darwin automata described in this paper provide a foundation for the development of intelligent machines that follow neurobiological rather than computational principles in their construction.

Acknowledgements

This work was supported by the W.M. Keck Foundation and the Neurosciences Research Foundation. We thank Jim Snook, Donald Hutson, and Doug Moore for their contribution to the design of Darwin VIII and Darwin IX, and our anonymous reviewers for useful comments.

Address correspondence to Anil K. Seth, W.M. Keck Laboratory, The Neurosciences Institute, 10640 John Jay Hopkins Drive, San Diego, CA 92121, USA. Email: seth@nsi.edu.

Anil K Seth

Anil Seth received a B.A. (Hons) in natural sciences from Cambridge University (1994), where he was awarded the Richards prize and elected a scholar of King's college three times. From Sussex University he obtained an M.Sc., with distinction, in knowledge-based systems (1996), and a D.Phil. in Computer Science and Artificial Intelligence (2000). He joined The Neurosciences Institute in 2001 as a Postdoctoral Fellow in theoretical neurobiology. His current interests include theoretical neuroanatomy, brain-based neural network modeling, and magnetic brain imaging.

Jeffrey L. McKinstry

Jeffrey L. McKinstry received his B.A. in Computer Science from Point Loma Nazarene University (1987). He received an M.S. in Computer Science from the University of Southern California in 1991. In 1999 he received a Ph.D. in Computer Engineering from the University of California, San Diego. His dissertation was entitled, "A model of Primary Visual Cortex: From Single Cells to Feature Maps". He is currently a Postdoctoral Fellow in theoretical neurobiology at The Neurosciences Institute in La Jolla, California and is a Professor of Computer Science at Point Loma Nazarene University in San Diego.

Gerald M. Edelman

Gerald M. Edelman, M.D., Ph.D., is Founder and Director of The Neurosciences Institute, a privately supported, not-for-profit center for research focused on

understanding the biological basis of higher brain functions in human beings. Edelman's early studies on the structure of antibodies while on the faculty of The Rockefeller University led to his being awarded the Nobel Prize for Physiology or Medicine in 1972. He later moved into the area of brain research where he has formulated a detailed theory to explain the development and organization of higher brain functions in terms of a process known as neuronal group selection or Neural Darwinism. In addition to the Nobel Prize, Dr. Edelman has been the recipient of numerous awards and honors, including many honorary degrees. He is a member of the National Academy of Sciences, the American Philosophical Society, and several foreign societies, including the Academy of Sciences, Institute of France. He is author of over 450 research publications.

Jeffrey L. Krichmar

Jeffrey L. Krichmar received a B.S. in Computer Science in 1983 from the University of Massachusetts at Amherst, a M.S. in Computer Science from The George Washington University in 1991, and a Ph.D. in Computational Sciences and Informatics from George Mason University in 1997. He spent 15 years as a software engineer on projects ranging from the PATRIOT Missile System at the Raytheon Corporation to Air Traffic Control for the Federal Systems Division of IBM. In 1997, he became an assistant professor at The Krasnow Institute for Advanced Study at George Mason University. In 1999, he became a research fellow at The Neurosciences Institute in San Diego where he is currently a Senior Fellow in Theoretical Neurobiology at The Neurosciences Institute. His research interests include biologically plausible models of learning and memory, the

effect of neural architecture on neural function, and testing theories of the nervous system with Brain-Based Devices that interact with the environment.

References

[1] A. Treisman, Feature binding, attention and object perception, *Philos Trans R Soc Lond B Biol Sci*, *353* (1373), 1998, 1295-306.

[2] N. Almassy, G. M. Edelman, and O. Sporns, Behavioral constraints in the development of neuronal properties: a cortical model embedded in a real-world device, *Cereb Cortex*, *8* (4), 1998, 346-61.

[3] G. M. Edelman, G. N. Reeke, W. E. Gall, G. Tononi, D. Williams, and O. Sporns, Synthetic neural modeling applied to a real-world artifact, *Proc Natl Acad Sci U S A*, *89* (15), 1992, 7267-71.

[4] J. L. Krichmar and G. M. Edelman, Machine psychology: autonomous behavior, perceptual categorization and conditioning in a brain-based device, *Cereb Cortex*, *12* (8), 2002, 818-30.

[5] J. L. McKinstry, A. K. Seth, G. M. Edelman, and J. L. Krichmar, Synchronous activity binds visual stimulus properties viewed by a brain-based device, *Soc. Neurosci Abst*2002, 558.12.

[6] A. K. Seth, J. L. McKinstry, G. M. Edelman, and J. L. Krichmar, Visual binding through reentrant connectivity and dynamic synchronization in a brain-based device, *Cereb Cortex*2003, Submitted.

[7] G. M. Edelman, *Neural Darwinism: The Theory of Neuronal Group Selection*. New York: Basic Books, Inc., 1987.

[8] H. P. Moravec, The Stanford cart and the CMU rover., *Proceedings of the IEEE*, *71* (7), 1983, 872-884.

[9] N. Nilsson, "Shakey the robot.," SRI International, Menlo Park, CA Technical Note 323, April 1984.

[10] O. Sporns and W. H. Alexander, Neuromodulation and plasticity in an autonomous robot, *Neural Networks*, *15* (4), 2002, 761-774.

[11] P. Verschure and T. Voegtlin, A bottom-up approach towards the acquisition and expression of sequential representations applied to a behaving real-world device, *Neural Networks*, *11* (7-8), 1998, 1531-1549.

[12] P. Verschure, Environmentally mediated synergy between perception and behaviour in mobile robots, *Nature*, *425*2003, 620-624.

[13] P. Fitzpatrick and G. Metta, Grounding vision through experimental manipulation, *Philos Transact Ser A Math Phys Eng Sci*, *361* (1811), 2003, 2165-85.

[14] P. Husbands, T. M. C. Smith, N. Jakobi, and M. O'Shea, Better living through chemistry: evolving GasNets for robot control, *Connection Science*, *10* (3-4), 1998, 185-210.

[15] R. Pfeifer and C. Scheier, Sensory-motor coordination: the metaphor and beyond, *Robotics and Autonomous Systems*, *20*1997, 157-178.

[16] A. R. Russell, "Using tactile whiskers to measure surface contours," in *Proc. IEEE International Conference on Robotics and Automation*, 1992, pp. 1295-1300.

[17] M. Kaneko, N. Kanayama, and T. Tsuji, Active antenna for contact sensing, *IEEE Transactions on Robotics and Automation*, *14* (2), 1998, 278-291.
[18] M. Fend, B. S., H. Yokoi, and R. Pfeifer, "An active artificial whisker array for texture discrimination," in *Proc. IEEE/RSJ International Conference on Intelligent Robots and Systems*, 2003.
[19] D. Jung and A. Zelinksy, "Whisker-based mobile robot navigation," in *Proc. IEEE/RSJ International Conference on Intelligent Robots and Systems*, 1996, pp. 497-504.
[20] R. A. Brooks, A robot that walks; emergent behavior from a carefully evolved network, *Neural Computation*, *1*1989, 252-262.
[21] C. von der Malsburg, A neural cocktail-party processor, *Biol. Cybern.*, *54*1986, 29-40.
[22] G. Tononi, O. Sporns, and G. M. Edelman, Reentry and the problem of integrating multiple cortical areas: simulation of dynamic integration in the visual system, *Cereb Cortex*, *2* (4), 1992, 310-35.
[23] G. M. Edelman, Neural Darwinism: selection and reentrant signaling in higher brain function, *Neuron*, *10* (2), 1993, 115-25.
[24] L. G. Ungerleider and J. V. Haxby, 'What' and 'where' in the human brain, *Curr Opin Neurobiol*, *4*1994, 157-165.
[25] W. Schultz, P. Dayan, and P. R. Montague, A neural substrate of prediction and reward, *Science*, *275* (5306), 1997, 1593-9.
[26] O. Sporns, N. Almassy, and G. M. Edelman, Plasticity in value systems and its role in adaptive behavior., *Adaptive Behavior*, *8* (2), 2000, 129-148.
[27] G. Aston-Jones and F. E. Bloom, Norepinephrine-containing locus coeruleus neurons in behaving rats exhibit pronounced responses to non-noxious environmental stimuli, *J Neurosci*, *1*1981, 887-900.
[28] J. Wray and G. M. Edelman, A model of color vision based on cortical reentry, *Cereb Cortex*, *6* (5), 1996, 701-716.
[29] E. L. Bienenstock, L. N. Cooper, and P. W. Munro, Theory for the development of neuron selectivity: orientation specificity and binocular interaction in visual cortex, *J Neurosci*, *2* (1), 1982, 32-48.
[30] S. Song and L. F. Abbott, Cortical development and remapping through spike timing-dependent plasticity, *Neuron*, *32* (2), 2001, 339-50.
[31] P. R. Montague, P. Dayan, and T. J. Sejnowski, A framework for mesencephalic dopamine systems based on predictive Hebbian learning, *J Neurosci*, *16* (5), 1996, 1936-47.
[32] K. J. Friston, G. Tononi, G. N. Reeke, Jr., O. Sporns, and G. M. Edelman, Value-dependent selection in the brain: simulation in a synthetic neural model, *Neuroscience*, *59* (2), 1994, 229-43.
[33] M. A. Harvey, R. Bermejo, and H. P. Zeigler, Discriminative whisking in the head-fixed rat: optoelectronic monitoring during tactile detection and discrimination tasks, *Somatosens Mot Res*, *18* (3), 2001, 211-22.
[34] T. Prigg, D. Goldreich, G. E. Carvell, and D. J. Simons, Texture discrimination and unit recordings in the rat whisker/barrel system, *Physiol Behav*, *77* (4-5), 2002, 671-5.

[35] T. A. Woolsey and H. Van der Loos, The structural organization of layer IV in the somatosensory region (SI) of mouse cerebral cortex. The description of a cortical field composed of discrete cytoarchitectonic units, *Brain Res*, *17* (2), 1970, 205-42.
[36] K. F. Jensen and H. P. Killackey, Terminal arbors of axons projecting to the somatosensory cortex of the adult rat. I. The normal morphology of specific thalamocortical afferents, *J Neurosci*, *7* (11), 1987, 3529-43.
[37] A. A. Ghazanfar and M. A. Nicolelis, Spatiotemporal properties of layer V neurons of the rat primary somatosensory cortex, *Cereb Cortex*, *9* (4), 1999, 348-61.
[38] S. Maren and M. S. Fanselow, The amygdala and fear conditioning: has the nut been cracked?, *Neuron*, *16* (2), 1996, 237-40.
[39] J. E. LeDoux, Emotion: clues from the brain, *Annu Rev Psychol*, *46*1995, 209-35.
[40] A. B. Saul and A. L. Humphrey, Evidence of input from lagged cells in the lateral geniculate nucleus to simple cells in cortical area 17 of the cat, *J Neurophysiol*, *68* (4), 1992, 1190-208.
[41] J. Wolfe and L. A. Palmer, Temporal diversity in the lateral geniculate nucleus of cat, *Vis Neurosci*, *15* (4), 1998, 653-75.
[42] N. J. Mackintosh, *Conditioning and associative learning*. Oxford: Oxford University Press, 1983.
[43] G. C. DeAngelis, I. Ohzawa, and R. D. Freeman, Receptive-field dynamics in the central visual pathways, *Trends Neurosci*, *18* (10), 1995, 451-8.
[44] A. Clark, *Being there: Putting brain, body, and world together again*. Cambridge, MA: MIT Press, 1997.
[45] K. Kawamura, C. A. Clifton, K. A. Hambuchen, and P. Ratanaswasd, "Multiagent based cognitive robot architecture and its realization: towards body-mind integration," in *Proc. IEEE Conference on Robotics and Automation*, 2004.
[46] D. Roy, K. Hsiao, and N. Mavridis, Mental imagery for a conversational robot, *IEEE Transactions on Systems, Man, and Cybernetics*(in press).
[47] S. S. M. Wang and P. M. Will, Sensors for computer controlled mechanical assembly, *Industrial Robot* (March), 1978, 9-18.
[48] G. M. Edelman and J. Gally, Degeneracy and complexity in biological systems, *Proc. Natl. Acad. Sci. USA*, *98* (24), 2001, 13763-13768.

Area	*Size*	*σ-fire*	*σ-phase*	*σ-vdep*	*ω*	*g*
V1 (6)	60x80	-	-	-	-	-
V2 (6)	30x40	0.10	0.45	0.05	0.30	1.0*
V4 (6)	15x20	0.20	0.45	0.10	0.50	1.0*
C	15x20	0.10	0.10	0.10	0.50	1.0
IT	30x30	0.20	0.20	0.10	0.75	1.0
S	4x4	0.10	0.00	0.00	0.15	1.0
Mic-right	1x1	-	-	-	-	-
Mic-left	1x1	-	-	-	-	-
A-left	4x4	0.00	0.00	0.10	0.50	1.0
A-right	4x4	0.00	0.00	0.10	0.50	1.0

Table 1. Darwin VIII neuronal unit parameters.

Projection	*Arbor*	*P*	$c_{ij}(0)$	*type*	η	θ_1	θ_2	*k1*	*k2*
V1→V2	[] 0x0	1.00	1,2	PI	0.00	0	0	0.00	0.00
V2→V2(intra)	[] 3x3	0.75	0.45,0.85	VD	0.00	0	0	0.00	0.00
V2→V2(inter) (X)	[] 2x2	0.40	0.5,0.65	VD	0.00	0	0	0.00	0.00
V2→V2(intra)	Θ 18,25	0.10	-0.05,-0.1	VI	0.00	0	0	0.00	0.00
V2→V2(inter)	[] 2x2	0.05	-0.05,-0.1	VI	0.00	0	0	0.00	0.00
V2→V4	[] 3x3	0.40	0.1,0.12	VI	0.00	0	0	0.00	0.00
V4→V2 (X)	[] 1x1	0.10	0.25,0.5	VD	0.00	0	0	0.00	0.00
V4→V4(inter) (X)	[] 2x2	0.40	1.75,2.75	VD	0.00	0	0	0.00	0.00
V4→V4(intra)	Θ 10,15	0.10	-0.15,-0.25	VI	0.00	0	0	0.00	0.00
V4→V4(inter)	Θ 10,15	0.10	-0.15,-0.25	VI	0.00	0	0	0.00	0.00
V4→V4(inter)	[] 2x2	0.03	-0.15,-0.25	VI	0.00	0	0	0.00	0.00
V4→C	[] 3x3	1.00	0.002,0.0025	VI	0.00	0	0	0.00	0.00
V4→IT	*special*	-	0.1,0.15	VI	0.00	0	0	0.00	0.00
IT→V4 (X)	non-topo	0.01	0.05,0.07	VD	0.00	0	0	0.00	0.00
IT→IT	non-topo	0.10	0.14,0.15	VD	0.10	0	0.866	0.90	0.45
IT→C #	non-topo	0.10	0.2,0.2	VD	1.00	0	0.707	0.45	0.65
IT→S #	non-topo	1.00	0.0005,0.001	VI	0.10	0	0.707	0.45	0.45
C→V4 (X)	non-topo	0.01	0.05,0.07	VD	0.00	0	0	0.00	0.00
C→C	Θ 6,12	0.50	-0.05,-0.15	PI	0.00	0	0	0.00	0.00
C→Mleft	non-topo	1.00	35,35	VD	0.00	0	0	0.00	0.00
C→Mright	non-topo	1.00	35,35	VD	0.00	0	0	0.00	0.00
S→C	non-topo	0.50	0.5,0.5	VD	0.00	0	0	0.00	0.00
S→S	non-topo	0.50	0.7,0.8	VD	0.00	0	0	0.00	0.00
A-left→C	left-only	1.00	0.5,0.5	VD	0.00	0	0	0.00	0.00
A-right→C	right-only	1.00	0.5,0.5	VD	0.00	0	0	0.00	0.00
A-left→C	right-only	1.00	-0.15,-0.15	PI	0.00	0	0	0.00	0.00
A-right→C	left-only	1.00	-0.15,-0.15	PI	0.00	0	0	0.00	0.00
A-left→S	non-topo	1.00	35,35	VD	0.00	0	0	0.00	0.00
A-right→S	non-topo	1.00	35,35	VD	0.00	0	0	0.00	0.00
A-left←→A-right	non-topo	1.00	-1,-1	PI	0.00	0	0	0.00	0.00
A-left←→A-right	non-topo	1.00	-0.5,-0.5	VD	0.00	0	0	0.00	0.00
Mic-left,Mic-right→A-left,A-right	non-topo	1.00	5,5	PI	0.00	0	0	0.00	0.00

Table 2. Properties of anatomical projections and connection types in Darwin VIII.

Side	*Whisker*	φ_w	$g_w\ (wd(t) > 0)$	$g_w\ (wd(t) \leq 0)$
Left	*BK*	*89*	*0.05*	*0.075*
	MD	*33*	*0.1*	*0.2*
Right	*BK*	*110*	*0.075*	*0.15*
	MD	*28*	*0.15*	*0.30*

Table 3. Wall-following parameters for Darwin IX.

Area	*Size*	σ-*fire*	σ-*phase*	σ-*vdep*	ω	*g*
Th (6)	1x20	0.3	-	-	0.8	-
S1 (6)	1x20	0.10	0.00	0.00	0.0	1.0
S2	30x30	0.20	0.00	0.00	0.8	1.0
S	1x1	-0.10	0.00	0.00	0.0	1.0
Amy	1x1	0.00	0.00	0.00	0.0	1.75
M_{ave}	3x6	0.00	0.00	0.00	0.0	1.0
FS	1x1	-	-	-	-	-

Table 4. Darwin IX neuronal unit parameters.

Projection	*Arbor*	*P*	$c_{ij}(0)$
Th→S1	[] 0x0	1.00	13.0,15.0
S1→S1(intra)	[] 2x8	1.00	-0.45,-0.60
S1→S2	*special*	-	0.25,0.25
FS→Amy	non-topo	1.00	5.0,5.0
Amy→ M_{ave}	non-topo	1.00	40.0,40.0
FS→ M_{ave}	non-topo	1.00	50.0,50.0
FS→S	non-topo	1.00	50.0,50.0
Amy→S	non-topo	1.00	-50.0,-50.0
S2→Amy	non-topo	1.00	0.0001,0.0003

Table 5. Properties of anatomical projections and connection types in Darwin IX.

Table 1. Values of parameters defining properties of neuronal units in Darwin VIII. Area *V1* is an input area and its activity is set based on the camera image. Areas *V1*, *V2*, and *V4* have 6 sub-areas each with neuronal units selective for colour (red, and green), and line orientation (0, 45, 90, and 135 degrees). *Mic-left* and *Mic-right* are input areas and their activity is set based on the microphone input. The table indicates the number of neuronal units in each area or sub-area (*size*). Neuronal units in each area apart from areas *VI, Mic-left,* and *Mic-right* have a specific firing threshold (σ-*fire*), a phase threshold (σ-*phase*), a threshold above which voltage-dependent connections can have an effect (σ-*vdep*), a persistence parameter (ω), and a scaling factor (g). Asterisks mark values that are set to 2.0 for Darwin VIII subjects with lesioned reentrant connections (see Table 2).

Table 2. Properties of anatomical projections and connection types in Darwin VIII. A pre-synaptic neuronal unit connects to a post-synaptic unit with a probability (P) and projection shape (Arbor) which can be rectangular "[]" with a height and width (h x w), doughnut shaped "Θ" with an inner and outer radius (r1, r2), left-only (right-only) with the pre-synaptic unit only projecting to the left (right) side of the post-synaptic area, or non-topographical "non-topo" where all pairs of pre-synaptic and post-synaptic neuronal units have an equal probability of being connected. The initial connection strengths, $c_{ij}(0)$, are set randomly within the range (min, max). Connections marked with "intra" denote those within a visual sub-area and connections marked with "inter" denote those between visual sub-areas. Inhibitory "inter" projections connect visual sub-areas responding to shape only or to colour only (e.g. *V4-red*↔*V4-green, V4-horizontal*↔*V4-vertical*), excitatory "inter" projections connect shape sub-areas to colour sub-areas (e.g. *V4-red*↔*V4-vertical*). Projections marked # are value-dependent. A connection type can be phase-independent/voltage-independent (PI), phase-dependent/voltage-independent (VI), or phase-dependent/voltage-dependent (VD). Non-zero values for η, θ_1, θ_2, k_1, *and* k_2 signify plastic connections. The connection from *V4* to *IT* was special in that a given neuronal unit in area *IT* was connected to three neuronal units randomly chosen from three different *V4* sub-areas.

Table 3. Wall-following parameters for Darwin IX. Scaling factors g_w and φ_w were chosen according the physical response characteristics of the whiskers in order to allow Darwin IX to follow walls at a distance appropriate for the detection of textures. Factor g_w varies according to the direction of the corresponding whisker deflection such that there is a bias in favor of turning towards a wall.

Table 4. Darwin IX neuronal unit parameters. Area *Th* consists of 6 separate 'barrel areas' which take input directly from the 3 whiskers in each column on each side of Darwin IX. Activity in area *FS* is triggered by detection of 'foot-shock' pads by Darwin IX's downward-facing IR sensor. Neuronal units in all other areas have parameters as described for Darwin VIII (see Table 1).

Table 5. Properties of anatomical projections and connection types in Darwin IX. Connections between pre- and post-synaptic units are specified by the same parameters as for Darwin VIII (see Table 2) apart from connections between *S1* and *S2*. All barrels of *S1* project to area *S2* such that each neuronal unit in *S2* takes input from 3 ipsilateral *S1* neuronal units, each of which is in a different barrel. All pathways are voltage-independent, and all are non-plastic except for *S2*→*Amy* for which η=1.4, ρ=6, $\theta_1 = \theta_2 = 0.1$, and $k1 = k2 = 0.45$.

Figure 1. Darwin VIII consists of a mobile base equipped with several sensors and effectors, and a neural simulation running on a remote cluster of computer workstations. The mobile base contains a radio modem to transmit status, IR sensor information, and auditory information to the computer workstations and to receive motor commands from the simulation. Video output from a CCD camera mounted on Darwin VIII is sent to the workstation via RF transmission. The CCD camera and the two microphones on either side of the camera provide sensory input to the neuronal simulation. An infrared (IR) sensor at the front of platform detects differences in surface reflectivity, triggering reflexive turns. All behavioural activity other than the IR reflexive turn is evoked by signals received from the neural simulation.

Figure 2. Neuroanatomy of Darwin VIII. The simulated nervous system contains 28 neuronal areas, 53,450 neuronal units, and ~1.7 million synaptic connections (see text for details). Projections marked with an 'X' are removed during lesion experiments. Inset shows the form of the BCM rule where synaptic change (Δc_{ij}) is a function of the phase difference between post- and pre-synaptic units (Δp) and two thresholds (θ_1 and θ_2).

Figure 3. Choosing a new firing rate and phase for a neuronal unit. Phases and activities of pre-synaptic neuronal units are convolved into either a uniform distribution for phase-independent inputs (see top row left) or a cosine tuning curve distribution for phase-dependent inputs (see top row middle and right). The input distributions are linearly summed to create an overall synaptic input distribution for the post-synaptic neuronal unit (see middle row). The neuronal unit's phase threshold is subtracted from the distribution and a new phase is chosen with a probability proportional to the resulting distribution (see bottom row). The new activity for the neuronal unit is the activity level at the new phase plus the phase threshold.

Figure 4. Experimental setup for Darwin VIII. Darwin VIII views objects on two of the walls of an arena. The area Darwin VIII explores (2.29m by 1.67m) is constrained by a boundary of reflective construction paper. Detection of this boundary by Darwin VIII's infrared sensor triggers a reflexive turn. When Darwin VIII breaks the beam from the IR emitter to the IR sensor, a tone is emitted is from the speaker.

Figure 5. Darwin VIII behaviour following conditioning. Three separate Darwin VIII subjects were conditioned prefer one of 4 target shapes ('rd' = red diamond, 'rs' = red square, 'gs' = green square, 'gd' = green diamond). Bars represent the mean percentage tracking time with error bars denoting the standard deviation. A. Darwin VIII subjects with intact reentrant connections tracked the targets (white bars) significantly more than the distracters (gray bars) for each target shape, averaging over all approaches. B. Subjects with reentrant connections intact (white bars) tracked targets significantly better than subjects with lesions only during testing (light gray bars), and subjects with lesions during both training and testing (black bars). Asterisks denote $p < 0.01$ using a paired sample nonparametric sign test).

Figure 6. Snapshot of Darwin VIII's neuronal unit activity during a behavioural experiment. The panels next to Darwin VIII show the activity and phase of selected neural areas (top row; *V2-red*, *V2-green*, *V2-vertical*, *V2-diagonal*, second row; *V4-red*, *V4-green*, *V4-vertical*, *V4-diagonal*, third row; *IT*, fourth row; *C* and *S*). Each pixel in each area represents the activity (brightness) and phase (colour) of a neuronal unit (colours were chosen from a pseudocolor map, there is no connection between the colour of the stimulus object and the colour representing the phases of neuronal responses). Neuronal units responding to the red diamond share a common phase (red-orange colour), whereas those responding to the green diamond share a different phase (blue-green colour).

Figure 7. Neural activity during conditioning for a single Darwin VIII subject, showing areas *S, IT,* and *C* during a single approach to a target shape (red diamond) at an early stage (left panels, time steps 750-1165), and at a late stage of conditioning (right panels, time steps 6775-7170). Shown in the panel for each neural area is the proportion of neuronal units at a particular phase, where phase is shown along the y-axis with a range of 0 to 2π, and a gray scale for the marks denotes the proportion of neuronal units at a specific phase (white represents no neuronal units, black represents the maximal proportion of neuronal units). The solid line at the bottom of each panel indicates cycles for which the tone was present. In the early approach area *S* is inactive until tone onset. After conditioning, areas *S, IT,* and *C* are in phase with visual system activity corresponding to the target (lower trace) well before tone onset.

Figure 8. Darwin IX morphology. **A**. Darwin IX with its left and right whisker arrays. The arrangement of a whisker array is shown in the inset. Each array has 7 whiskers arranged in a row of 5 and a column of 3. Whiskers used for wall following are marked in green (FT,MD,BK). Whiskers that provide input to the neural simulation are marked in red. Note that one whisker (red/green) is used for both purposes. Whiskers marked in black are not used in the present model. **B**. Detail of a whisker array: The top (T), middle (M), and bottom (B) whiskers in the column provide input to the neural simulation. **C.** Schematic of textures *T1* and *T2*. Each texture consists of pegs embedded in a wall; pegs are aligned in rows corresponding to the whiskers in a column. Pegs in the top row deflect the top whisker (T), and similarly for pegs in the middle row (M) and the bottom row (B).

Figure 9. Global neuroanatomy of Darwin IX. The simulated nervous system contains 17 neuronal areas, 1161 neuronal units, and ~8400 synaptic connections. Aversive freezing/escape responses are evoked by activity in area M_{ave}. Areas $ThL_{T/M/B}$ *and* $ThR_{T/M/B}$ recieve input from the corresponding whiskers in the whisker columns on the appropriate side. These areas contain 'lag cells' with temporal response properties. The operation of two idealized lag cells (A and B) is shown in the inset. The post-stimulus internal state of cell A (s_A^{in}) rises quickly (gray dashed line), at a rate determined by φ_A. The internal state of B (s_B^{in}) rises more slowly (black dashed line, φ_B). When the internal state of each cell reaches a threshold (σ^{fire}), output is generated (solid lines) which decays at a rate determined by ω.

Figure 10. Experimental setup for Darwin IX. Darwin IX explored a walled enclosure (2.41m x 2.95m) with textures *T1* (vertically aligned pegs) and *T2* (vertically staggered pegs) on the walls. Instances of each texture were regularly spaced along the walls at intervals of ~30cm. Located on the floor adjacent to *T1* patterns were 'foot-shock' pads made of reflective construction paper. During training, detection of these pads by Darwin IX's downward-facing infrared sensor triggers an innate freezing/escape response. During testing, the pads were removed. Training and testing was repeated for each Darwin IX subject after exchanging the positions of *T1* and *T2*.

Figure 11. Conditioned aversion to textures by Darwin IX. The line tracings show the trajectory of a single Darwin IX subject during aversive conditioning to texture *T1* (left), and during testing (right). Large black dots show locations of aversive responses, gray shading show locations of *T1*. During testing all freezing/escape responses occurred in proximity to the aversive texture *T1*.

Figure 12. Spatiotemporal response properties of neuronal units in *S2*. The top panels show *S2* activity during two separate encounters (*a,b*) with texture *T1* by Darwin IX's left whisker column. The bottom panels show encounters of the same whiskers with texture *T2*. Each panel shows the activity of the 30x30 matrix of *S2* neuronal units (*x* and *y* axes) over 60 post-stimulus cycles (indicated by the *z* axis as well as by the colour scale). Neuronal units are shown if their activity exceeded a threshold (0.25)**.**

Figure 13. Similarity over time between pairwise combinations of activity patterns shown in Fig. 12, calculated as $sim(i, j) = v_i(t) \bullet v_j(t)$ where $v_i(t)$ is the normalized neuronal unit activity vector for pattern *i* at time *t.* Patterns representing the same texture are highly similar over time (black solid lines; *sim*(*T1*a,*T1*b), *sim*(*T2*a,*T2*b)), but patterns representing different textures are not similar (gray dashed lines; *sim*(*T1*a,*T2*a), *sim*(*T1*a,*T2*b), *sim*(*T2*a,*T1*a), *sim*(*T2*a,*T1*b)).

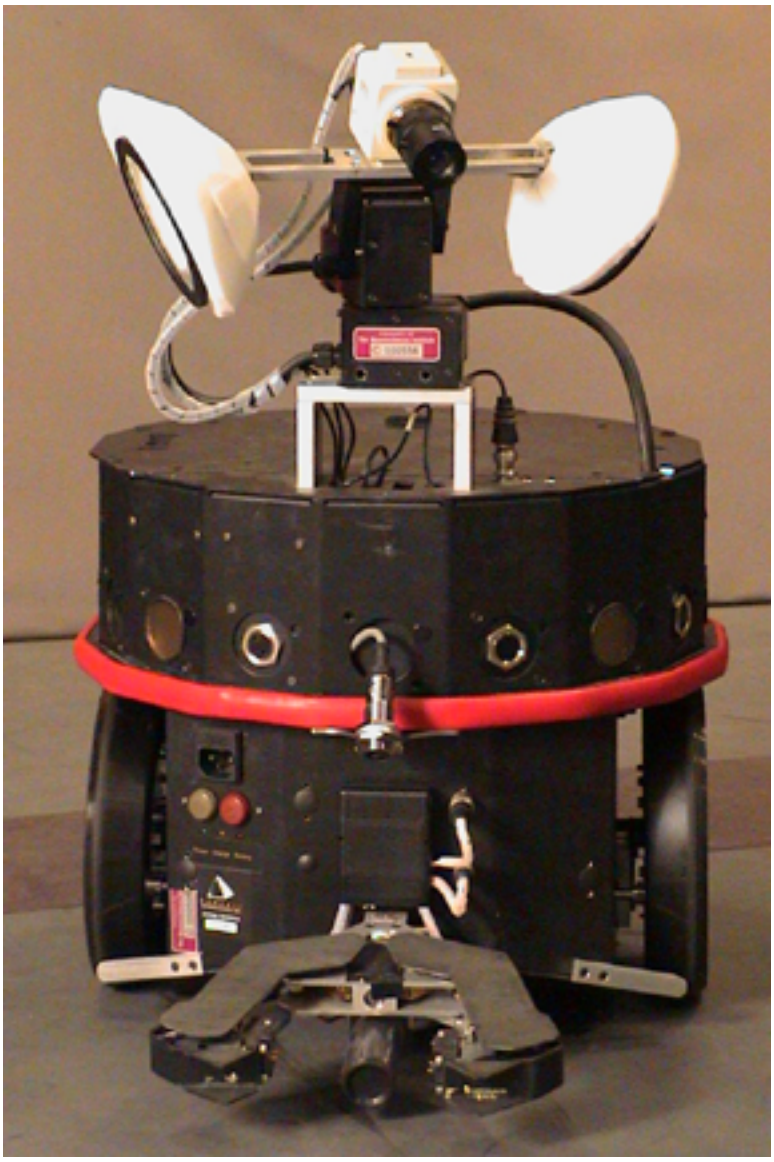

Figure 1

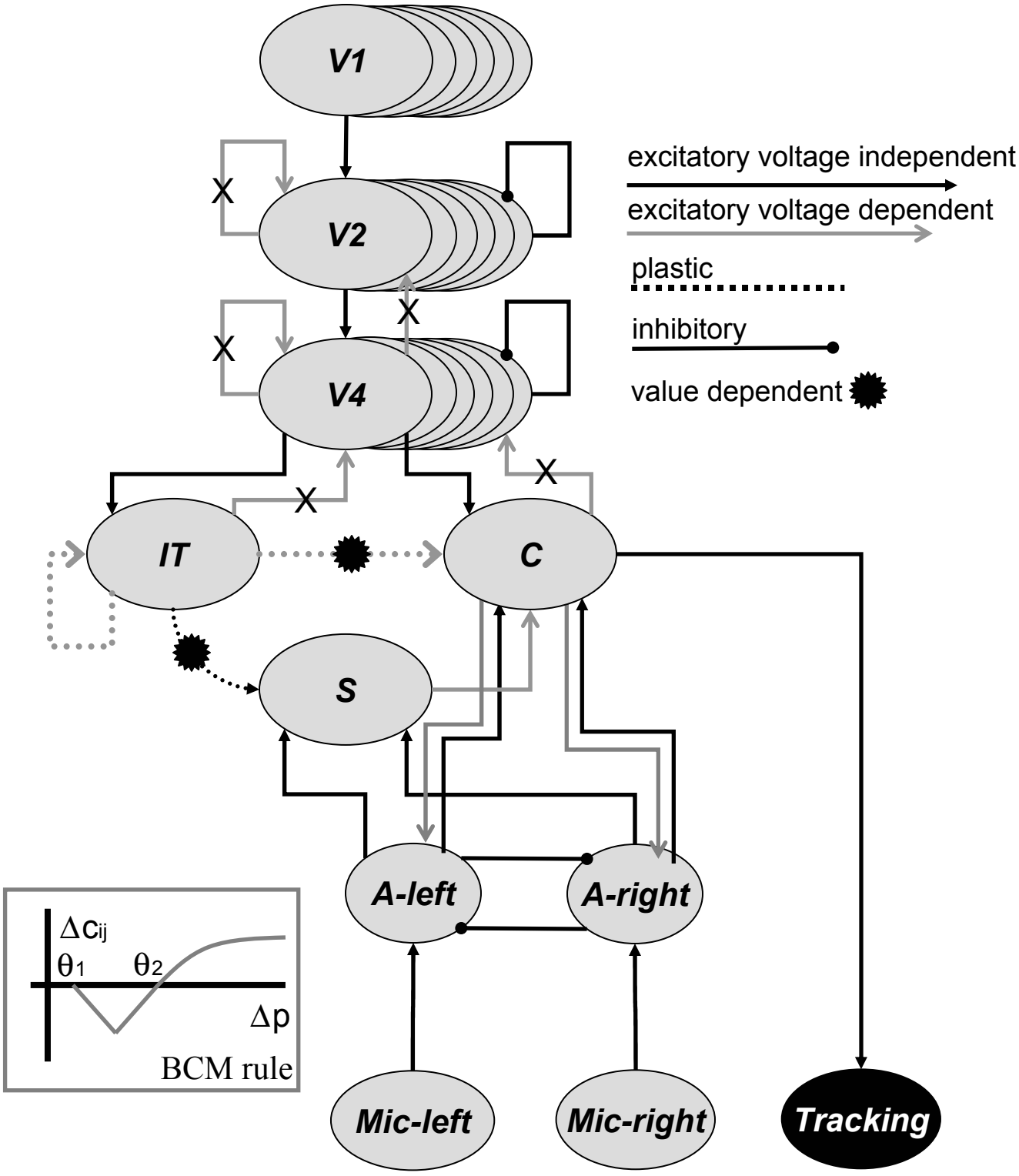
V1
V2
V4
IT
C
S
A-left
A-right
Mic-left
Mic-right
Tracking
excitatory voltage independent
excitatory voltage dependent
plastic
inhibitory
value dependent
X
Δcij
θ1
θ2
Δp
BCM rule

Figure 2

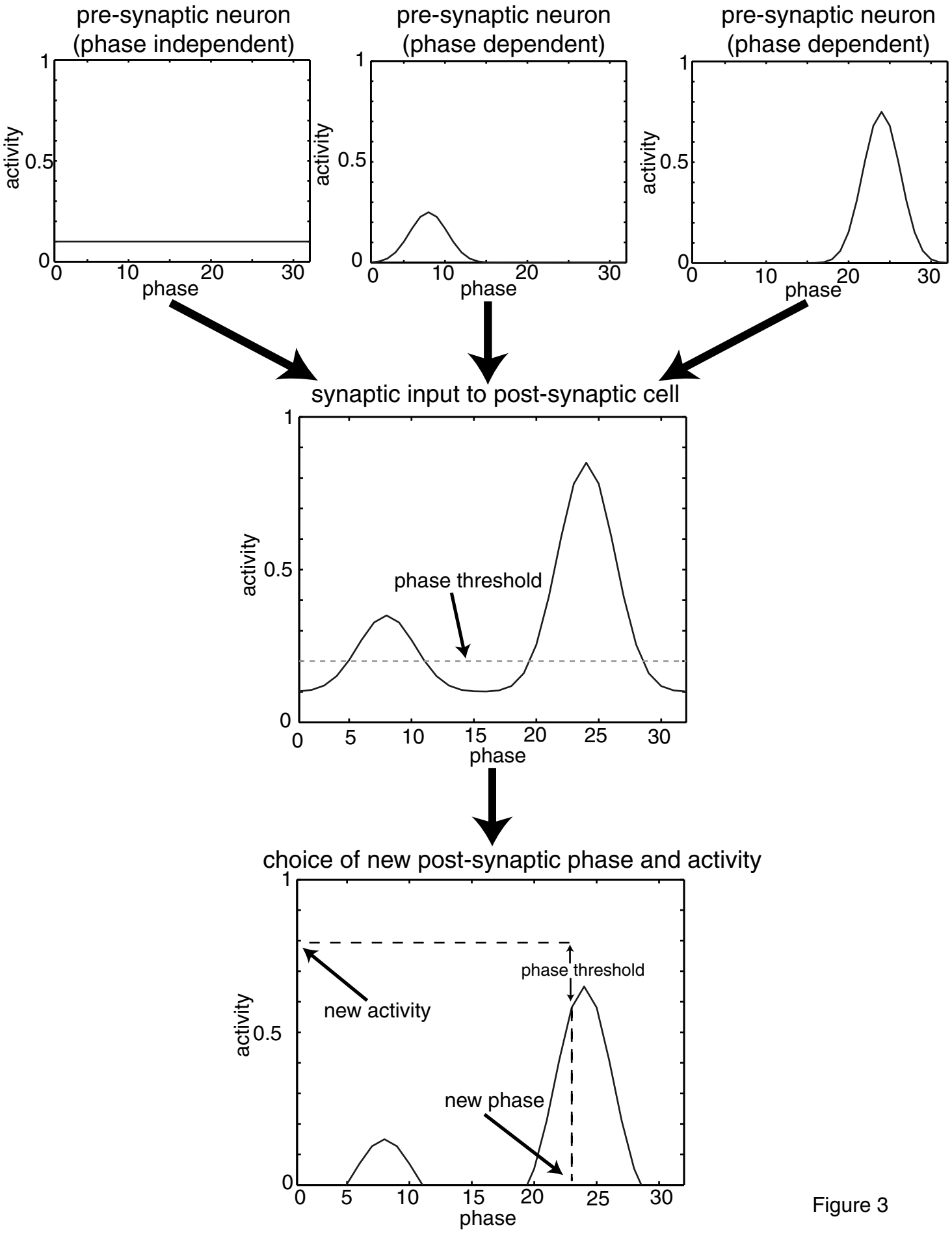
pre-synaptic neuron
(phase independent)
pre-synaptic neuron
(phase dependent)
pre-synaptic neuron
(phase dependent)
activity
phase
synaptic input to post-synaptic cell
phase threshold
choice of new post-synaptic phase and activity
new activity
new phase

Figure 3

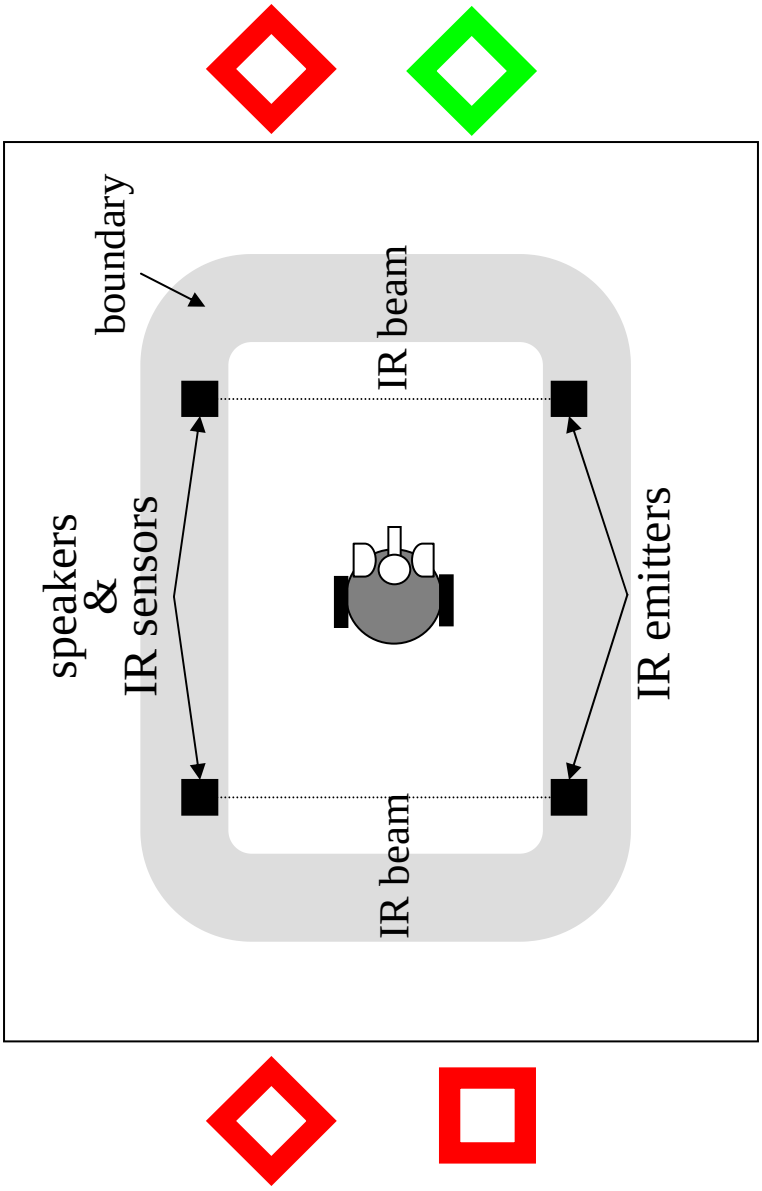

Figure 4

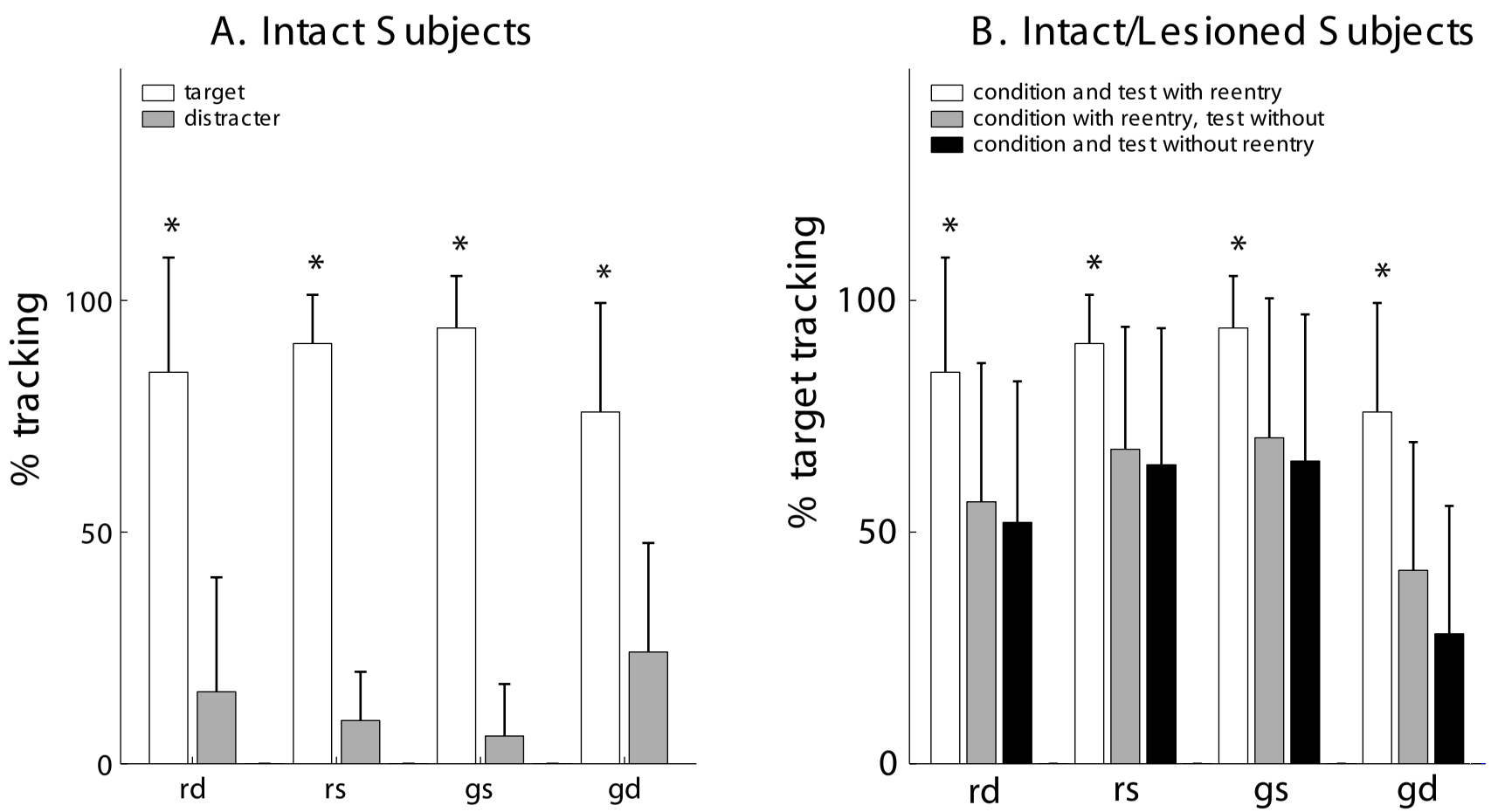
A. Intact Subjects
target
distracter
% tracking
100
50
0
rd
rs
gs
gd
B. Intact/Lesioned Subjects
condition and test with reentry
condition with reentry, test without
condition and test without reentry
% target tracking
100
50
0
rd
rs
gs
gd

Figure 5

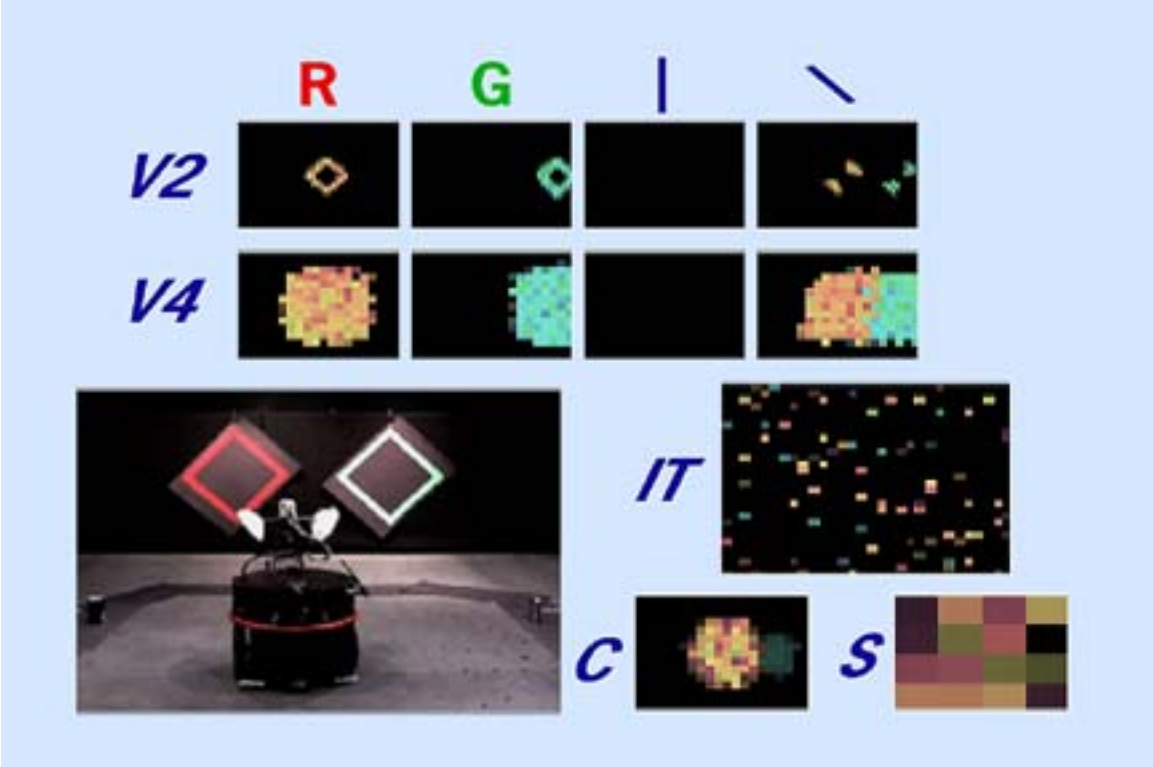

Figure 6

Early Conditioning
Late Conditioning
S
IT
C
phase
10
20
30
800
1115
6825
7120
timesteps

Figure 7

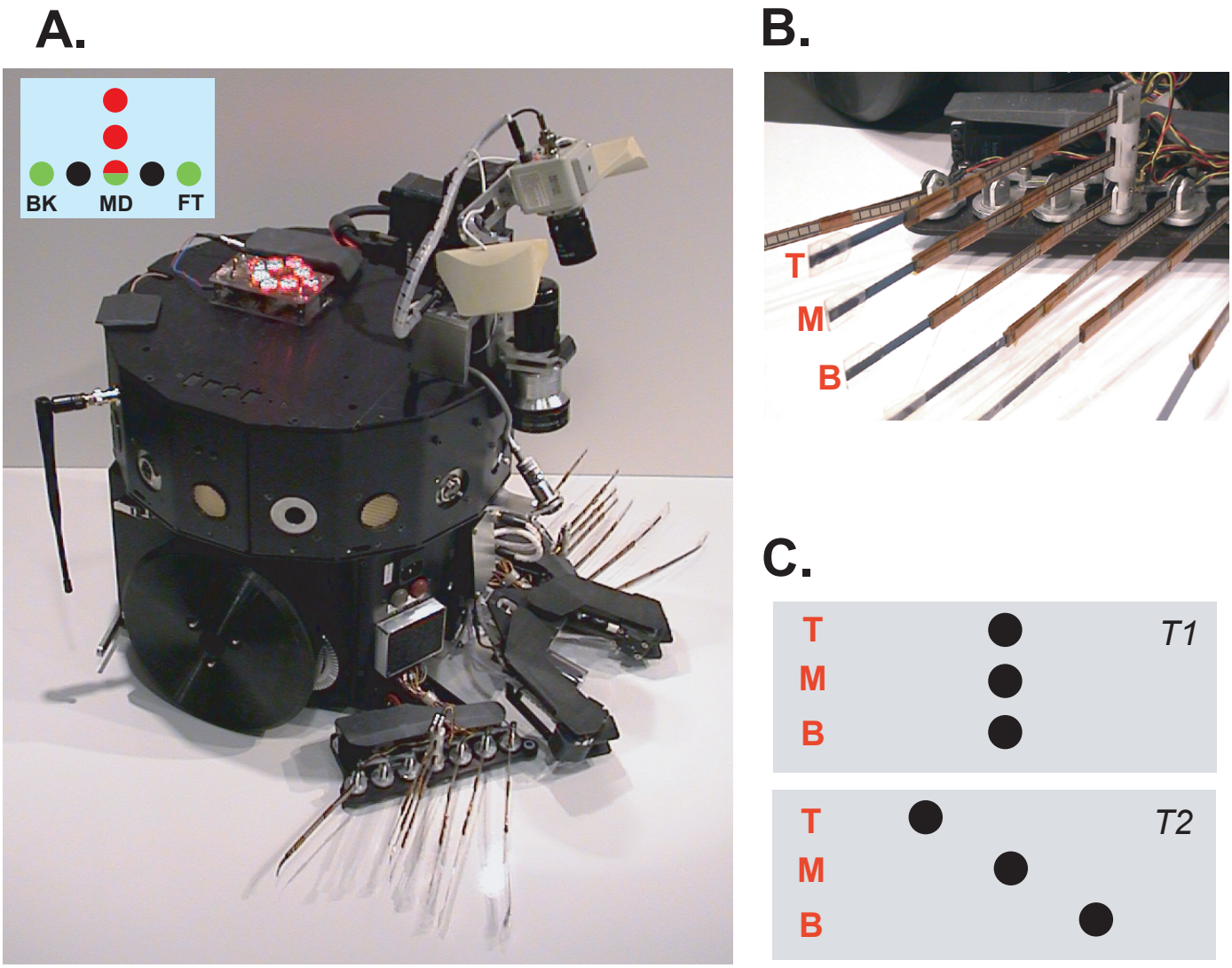

Figure 8

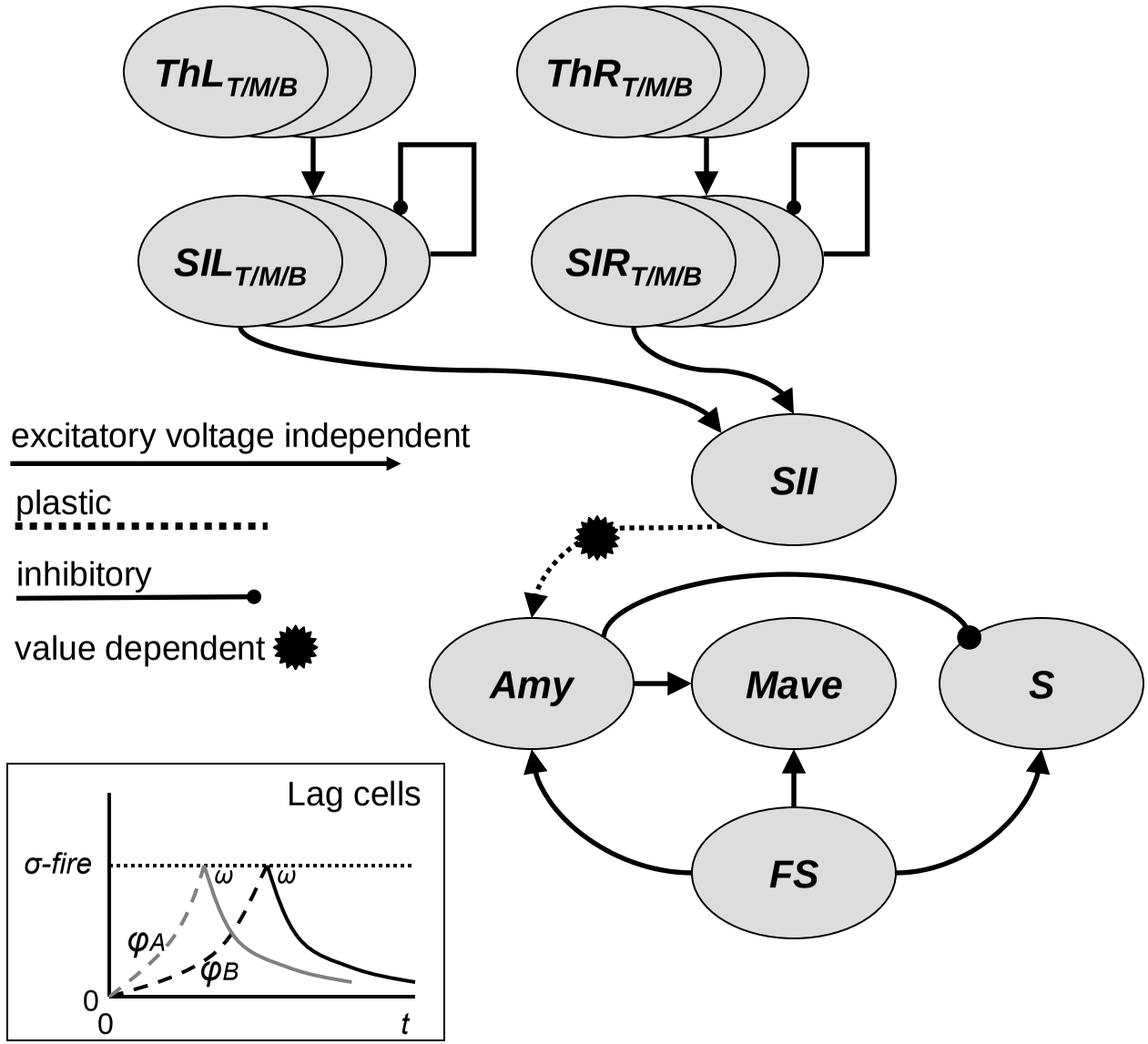
ThL T/M/B
ThR T/M/B
SIL T/M/B
SIR T/M/B
SII
excitatory voltage independent
plastic
inhibitory
value dependent
Amy
Mave
S
FS
Lag cells
σ-fire
ω
ω
φA
φB
0
0
t

Figure 9

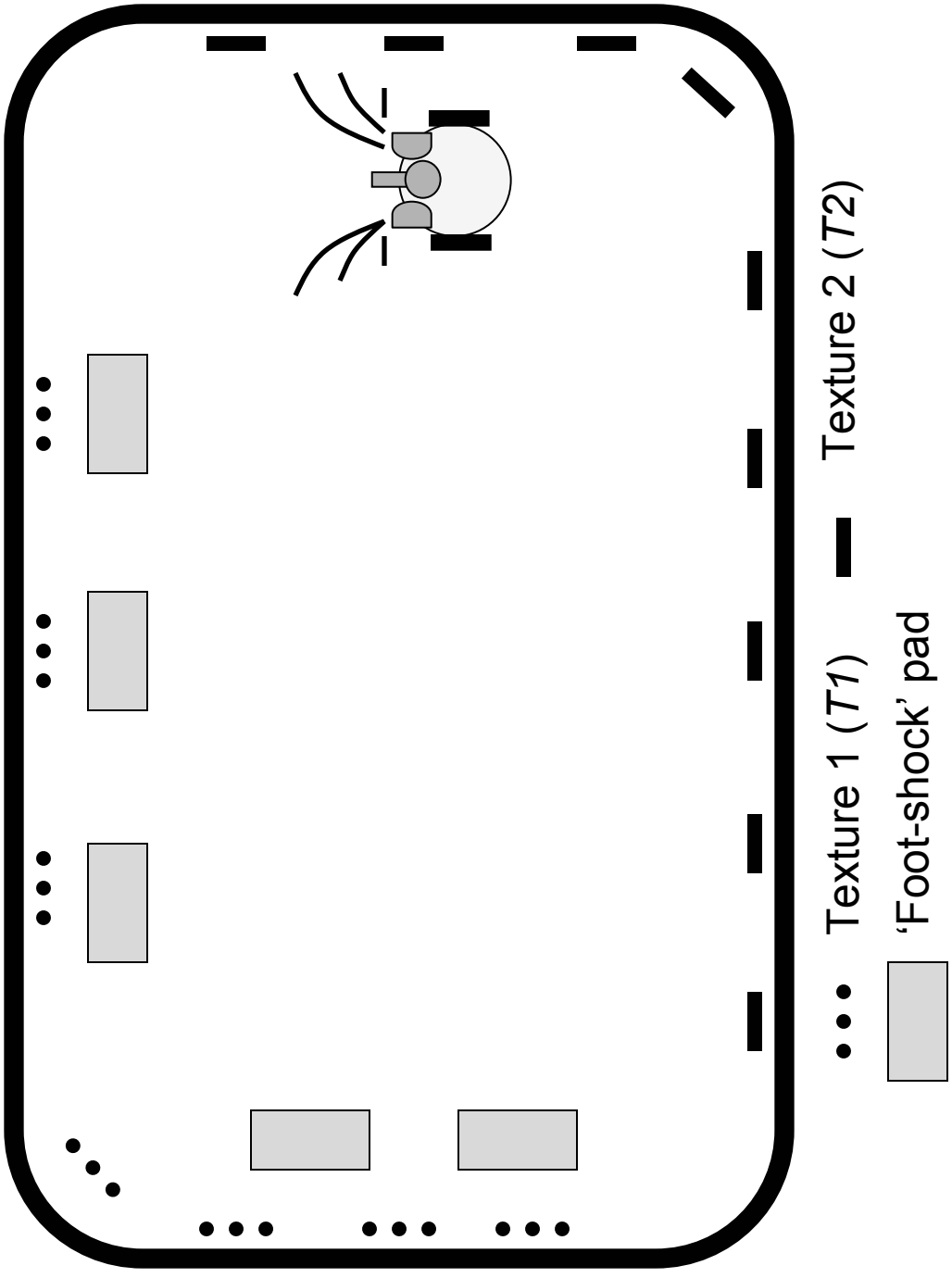

Figure 10

Figure 11

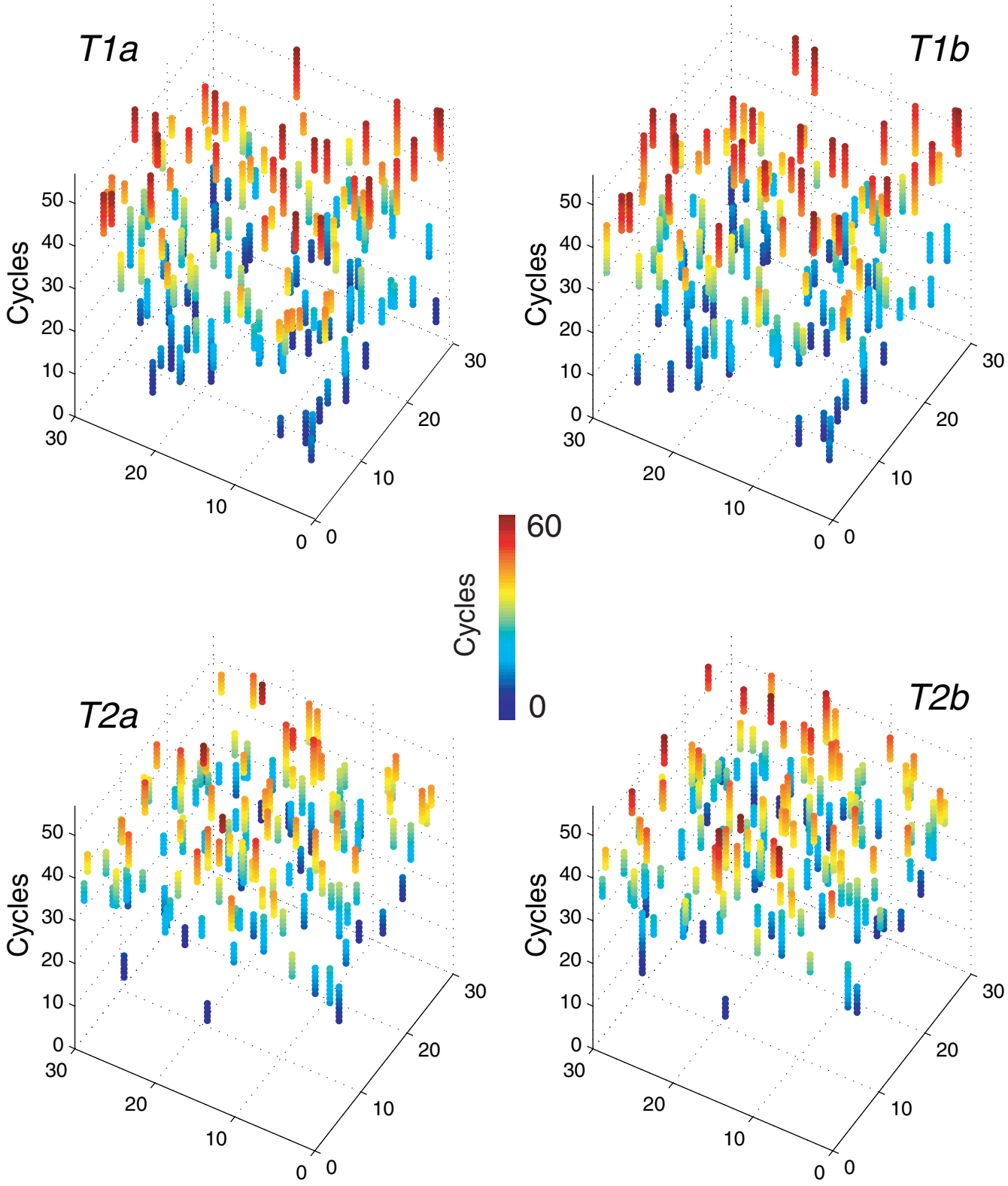

Figure 12

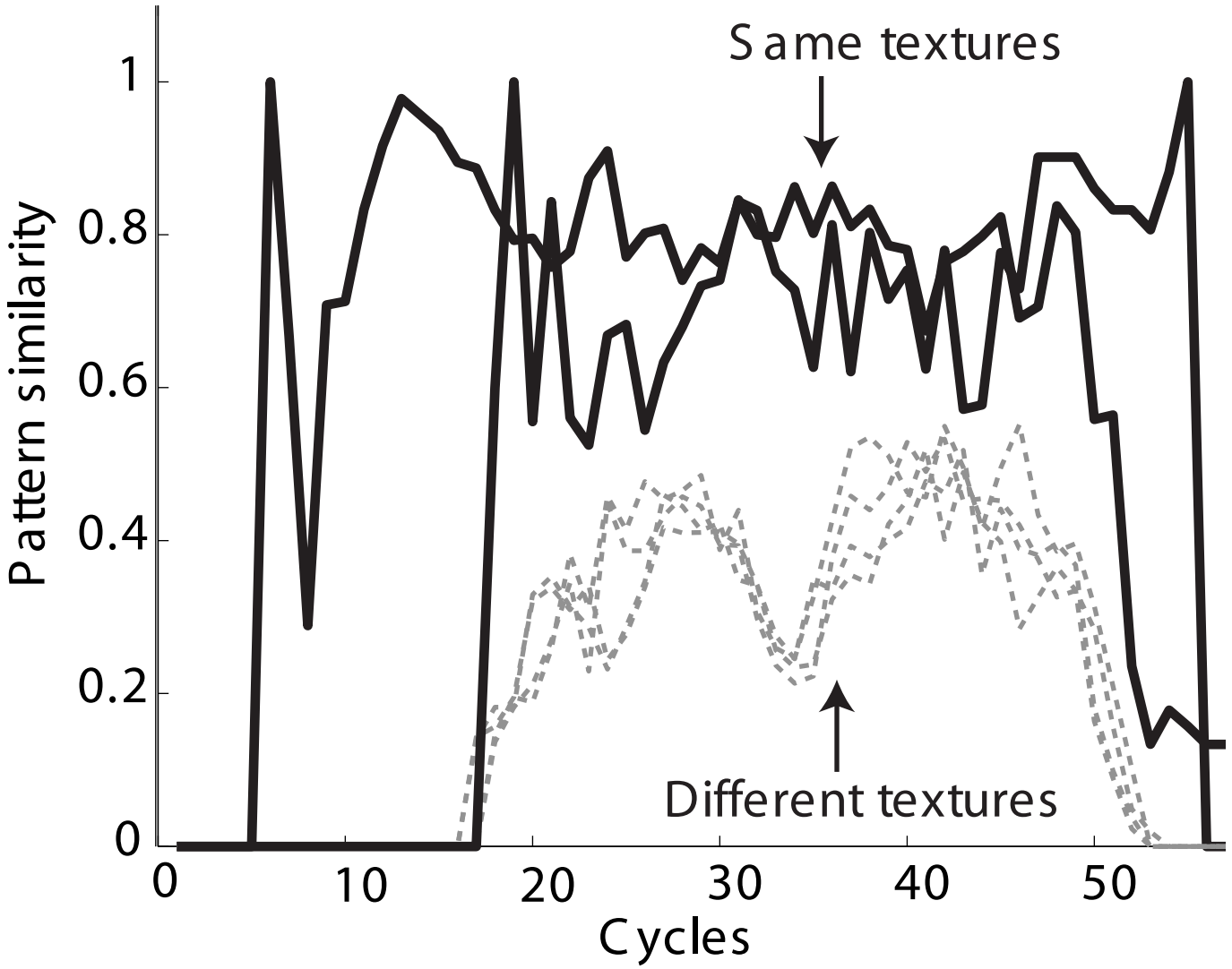
Same textures
Different textures
Pattern similarity
Cycles
0
0.2
0.4
0.6
0.8
1
0
10
20
30
40
50

Figure 13